

Performance Verification of the Raptor Guard

Installed in Sub Transmission Systems

by

Zui Chen

A Thesis Presented in Partial Fulfillment
of the Requirements for the Degree
Master of Science

Approved November 2016 by the
Graduate Supervisory Committee:

Ravi Gorur, Chair
George Karady
Keith Holbert

ARIZONA STATE UNIVERSITY

December 2016

ABSTRACT

In sub transmission systems, many more raptor deaths have been recorded near metal poles rather than wood poles. The metal pole, which is reliable in structure but also grounded, may increase the risk of electrocution when raptors perch on the insulator. This thesis focuses on evaluating the effectiveness of the raptor guard to prevent both debilitating and lethal electrocutions to local wildlife in 69 kV sub transmission systems. First, the two-dimensional (2D) finite difference methods (FDM) were proposed to solve the Poisson and Laplace equations, which describe the electric field. Second, the verification of the FDM algorithm was made based on a parallel-plate capacitor model. Then, the potential and the electric field were simulated by the raptor-insulator model to evaluate the possibility of flashover and leakage current under various conceivable scenarios. Third, several dielectric performance experiments were implemented to gain insight into the physical property of the raptor guard developed by the Salt River Project (SRP) as an example. The proposed initial-tracking-voltage and time-to-track experiments tested the ability of the guard, which is designed to prevent the tracking phenomenon under a contaminated situation such as rain, fog and snow. A data acquisition also collected the leakage current data for the comparison of maximum raptor tolerance. Furthermore, the puncture voltage of this guard material was performed by the dielectric breakdown voltage experiment in an oil-covered container. With the combination of the model simulation and the experiments in this research, the raptor guard was proven to be practical and beneficial in sub transmission system.

ACKNOWLEDGMENTS

First and foremost, I am thankful all the help, guidance, and support provided throughout this thesis work by Dr. Ravi Gorur. I would also like to thank Dr. George Karady and Dr. Keith E. Holbert for their time and consideration in being a part of my supervisory committee. Under the sponsorship of Salt River Project and the assistance from Mr. James Hunt and Michael Dyer, this project was able to be finished completely. Besides, the continual inspiration of my parents and close friends plays a vital role on the pathway to pursue my utmost goals, too. Last but not least, I do thank Arizona State University for bestowing the great opportunity to advance my scholastic experience.

For all, I am deeply grateful.

TABLE OF CONTENTS

	Page
LIST OF TABLES.....	vi
LIST OF FIGURES	vii
CHAPTER	
1 STUDY BACKGROUND.....	1
1.1 The Purpose of Raptor Protection	1
1.2 Raptor Type Description	3
1.3 Raptor Guard Description	4
2 FINITE DIFFERENCE METHOD	7
2.1 Introduction	7
2.2 Finite Difference and Difference Quotient.....	7
2.3 Construction of the Finite Difference Format	10
2.4 Difference Format of the Boundary Condition	12
2.4.1 Material Interface Overlap the Network Line.....	13
2.4.2 Material Interface on the Diagonal of Network.....	14
2.4.3 Nodes at the Interface Corner	15
2.4.4 Purely Capacitive Media vs. Conductive Media.....	16
2.5 Solution for Difference Equation Group.....	17
2.6 Simulation Flow Chart	18
3 RAPTOR-INSULATOR MODEL SIMULATION	21
3.1 FDM Code Validation.....	21

CHAPTER	Page
3.1.1 Capacitor Model with Different Length between Two Plates	21
3.1.2 Capacitor Model Inserted by Two Different Material	26
3.2 Insulator Model ----Shed Model vs. Bar Model.....	28
3.3 Raptor-Insulator Model	32
3.4 Parameter Setting	34
3.5 Case Classification	38
3.5.1 Case#1: Left Wing Contact Pole, Right Wing 3 Inches from Conductor....	38
3.5.2 Case#2: Left Wing 3 Inches from Pole, Right Wing Contact Conductor....	39
3.5.3 Case#3: Left Wing Contact Guard, Right Wing Contact Conductor.....	41
3.5.4 Wet and Dry Comparison	42
3.6 Result Summary	45
4 EXPERIMENT ON RAPTOR GUARD MATERIAL	46
4.1 Initial Tracking Voltage Test (ATSM D2303-13)	46
4.1.1 Circuit Diagram	46
4.1.2 Test Specimens	47
4.1.3 Specimens' Holder and Irrigation System	48
4.1.4 Procedure	51
4.1.5 Experimental Observation	52
4.1.6 Significance and Use.....	54
4.2 Time to Track Experiment (ATSM D2303-13)	55
4.3 Dielectric Breakdown Voltage Experiment.	61
4.3.1 System Diagram.....	62

CHAPTER	Page
4.3.2 Sample Holder and Electrode	62
4.3.3 Experiment Procedure.....	64
4.3.4 Experiment Result.....	65
4.4 Voltage Tolerance Test on the Golden Eagle.....	66
5 CONCLUSION AND FUTURE WORK.....	69
5.1 Conclusion.....	69
5.2 Future Work	70
5.2.1 Slit Problem between Two Boards	70
5.2.2 Simulation Efficiency	72
5.2.3 3D Model	72
REFERENCES	73
A CODE FOR CAPACITOR MODEL	76
B CODE FOR RAPATOR-INSULATOR MODEL	79
C CODE FOR LEAKAGE CURRENT DATA ANALYSIS.....	83

LIST OF TABLES

Table	Page
1.1 Raptor Body Measurement	3
3.1 Potential Matrix Corresponding to Figure 3.1.6	27
3.2 Shed Insulator Model Parameters	29
3.3 Raptor Model Parameter Setting.....	36
3.4 Simulation Summary.	45
4.1 Flow Rate Setting.....	48
4.2 ITV Result.....	55
4.3 TTT Result	55
4.4 TTT Leakage Current and Surface Resistance	61
4.5 Step Voltage Setting	65
4.6 Result of the Molted Golden Eagle Wing Feathers	66
4.7 Current of Golden Eagle When Electrodes Attached on Wing Joints	67
4.8 Current of Golden Eagle When Electrodes Attached on Toes	67

LIST OF FIGURES

Figure	Page
1.1.1 69 kV Horizontal Post Insulator Problem Design.....	2
1.2.1 Critical Dimension of the Gold Eagle.....	4
1.3.1 Guard's Slat Adjustment.....	6
1.3.2 Raptor Guard Installation.....	6
2.2.1 Point B Forward, Backward and Central Difference Quotient	9
2.3.1 Objective Field Discretization by Five-points Finite Difference Method	11
2.4.1 Material Interface Overlaps the Vertical Network Line	13
2.4.2 Material Interface Overlaps the Horizontal Grid Line.....	14
2.4.3 Node at Interface Corner.....	15
2.6.1 FDM Code Flow Chart in MATLAB	19
3.1.1 Simple Capacitor Model with Adjustable Plate Distance.....	21
3.1.2 Potential Distribution in Vertical Direction with Various Gap Distance	22
3.1.3 Electric Field in Vertical Direction with Various Gap Distance	24
3.1.4 Potential Contour for Gap= 3 cm.....	25
3.1.5 Potential Contour for Gap = 10 cm.....	25
3.1.6 Two Materials Inserted into A Capacitor.....	26
3.1.7 Potential Contour	27
3.2.1 Shed Insulator Model Example in 69 kV System.....	28
3.2.2 Potential along Shed Insulator	29
3.2.3 Electric Field along Shed Insulator.....	30
3.2.4 Bar Insulator Model Example in 69 kV System	31

Figure	Page
3.2.5 Potential along Bar Insulator	31
3.2.6 Electric Field along Bar Insulator	31
3.3.1 Line Post Insulator Parameter	33
3.3.2 Raptor Model Diagram with Detailed Dimension	34
3.4.1 Human Bio-Impedance under 60 Hz	35
3.4.2 Boundary Condition Numbering and Category	37
3.4.3 Boundary Condition Numbering and Category for Conductor.....	37
3.5.1 Case#1 Diagram.....	38
3.5.2 Pole Surface Vertical EF in Case#1	39
3.5.3 Insulator Surface Horizontal EF in Case#1	39
3.5.4 Case#2 Diagram.....	40
3.5.5 Pole Surface Vertical EF in Case#2.....	40
3.5.6 Insulator Surface Horizontal EF in Case#2	41
3.5.7 Case#3 Diagram.....	41
3.5.8 Pole Surface Vertical EF in Case#3.....	42
3.5.9 Insulator Surface Horizontal EF in Case#3	42
3.5.10 Wet Condition Diagram.....	43
3.5.11 Insulator Surface Horizontal Electric Field in Dry Condition	43
3.5.12 Insulator Surface Horizontal Electric Field in Wet Condition.....	44
3.5.13 Pole Surface Vertical Electric Field in Dry Condition	44
3.5.14 Pole Surface Vertical Electric Field in Wet Condition.....	45
4.1.1 ITV Circuit Diagram.....	46

Figure	Page
4.1.2 Raptor Sample Dimension	47
4.1.3 Top Electrode Diagram	49
4.1.4 Bottom Electrode Diagram	49
4.1.5 Filter Paper Dimension	50
4.1.6 Top Electrode Assembly	50
4.1.7 Holder and Irrigation System Assembly	51
4.1.8 Tracking during Experiment	53
4.1.9 Raptor Guard Sample after Burning	53
4.1.10 Black Fluffy Fibers on Surface	54
4.1.11 Tested Sample under Different Period and Voltage	54
4.2.1 NI USB-6008	57
4.2.2 RMS Leakage Current Data under 750 V	58
4.2.3 RMS Leakage Current Data under 1250 V	58
4.2.4 Surface Resistance Current Data under 750 V	59
4.2.5 Surface Resistance Data under 1250 V	60
4.3.1 Container for Dielectric Oil	62
4.3.2 Sample Attached on Ground Plate	63
4.3.3 Energized Top Electrode with A Spherical Contact	63
4.3.4 Sample in the Dielectric Oil	64
4.3.5 Voltage Step Profile	65
4.4.1 Raptor Bio-Impedance Estimation between Toes	68
5.2.1 Slit at the Junction	70

Figure	Page
5.2.2 Flashover Experiment Diagram	71

1 STUDY BACKGROUND

1.1 The Purpose of Raptor Protection

Raptors are a major problem for electrical utilities. They collide with overhead structures, contaminate insulators and equipment, and damage facilities leading to customer interruptions and bird fatalities. Their size, type, and habitat all contribute to the potential impact on the power grid [1] - [2].

On the sub transmission lines, birds are responsible for nearly 25% of all outages in the US. A 1990 survey reported that 86% of utilities indicated birds caused major problems [3]. Birds contact conductors while flying in or out, contaminate insulators leading to outages, and necessitate insulator replacement. These problems led to the formation of a task force within IEEE working group on insulator contamination and dielectric aging, whose objective was to provide recommended practices to mitigate bird-related outages.

The Edison Electric Institute identified reasons why birds are attracted to power lines. The pole increases their range of vision and attack speed when hunting; they also provide good hunting and roosting platforms. Nevertheless, more and more metal poles replaced wood poles. They are stronger, more durable, more economical in the long-term, and well-grounded. Compared with the wing span of adult birds like eagles, red-tailed hawks, etc., the relatively identical separation between conductors and conductors-to-ground is one of the leading causes of electrocution.

Electrical companies have begun to investigate means to minimize these negative impacts. There are several common electrocution-prevention methods that local units have come up with, which include the following: bird flight diverters, double deadened

structures, and insulated covers [3] – [6]. These especially apply to more than 8000 species of protected migratory birds in north America.

To justify the continual use of metal poles over wood for power reliability and to prevent a political storm on the negative environmental impact on the animal life, this study will review the raptor guard intended for reducing bird-related problems. The study focused on the 69 kV sub transmission system.

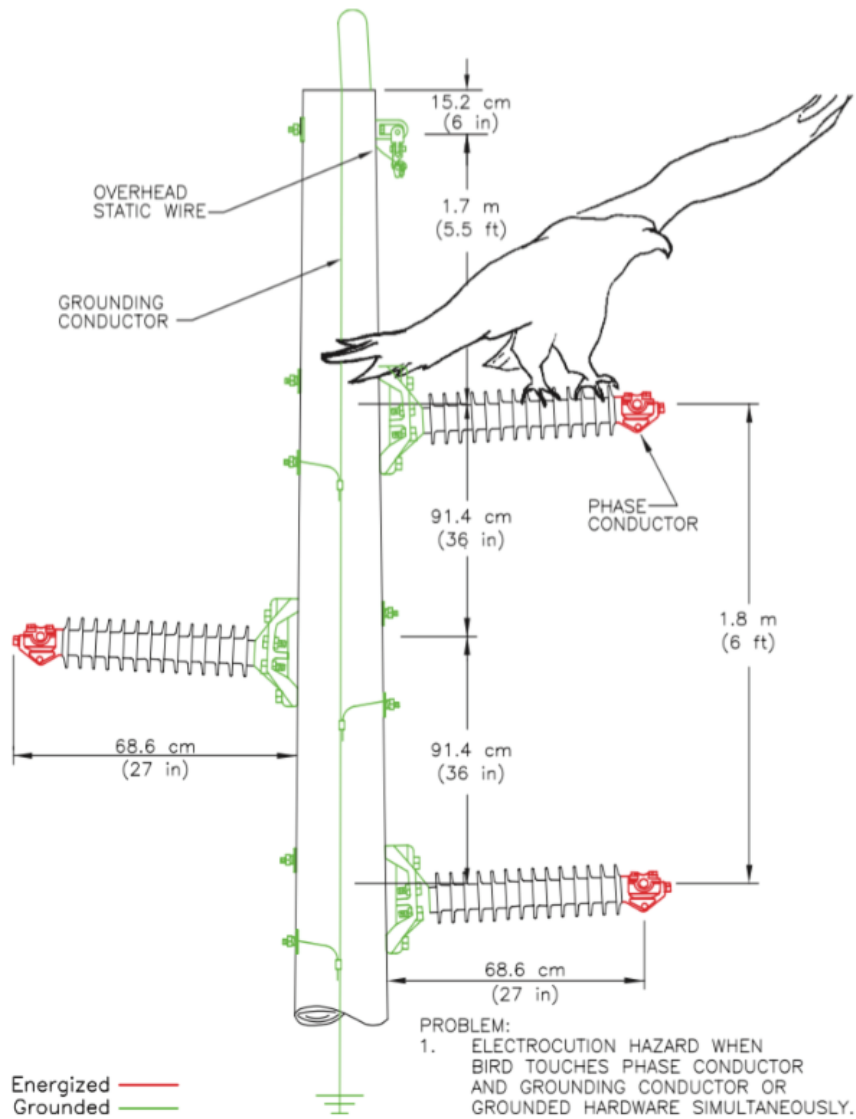


Figure 1.1.1 69 kV Horizontal Post Insulator Problem Design.

1.2 Raptor Type Description

In the Avian Power Line Interaction Committee study [3], over 15 types of raptors are under investigation (Table 1.1 and Figure 1.2.1). However, only the red-tailed hawk is considered in this study due to its regional distribution.

In Phoenix and most Arizona areas, the primary fatalities of huge birds are attributed to the red-tailed hawk, which is a mid-size raptor with roughly 125 cm wingspan. Though the wrist-to-wrist length for this raptor ranges from 36 to 58 cm, it is close to the insulator length in the sub transmission system [3]. For most raptors only perching on the insulator or the same conductor, there should be no danger for them since the potential on their body is within a safe range. However, for those raptors with enormous body sizes like red-tail hawks, their wings and twists could build a bridge between a bare conductor and a well-grounded pole, resulting in electrocution and fault current flow through it.

Table 1.1 Raptor Body Measurement

Species	Wrist-to-wrist cm (in) [sample size] [†]	Wingspan cm (in)	Height cm (in) [sample size] [§]
Turkey Vulture	58–61 (23–24) [n=2]	165–178 (65–70)	36–53 (14–21) [n=3]
Black Vulture		137–160 (54–63)	
California Condor		249–300 (98–118)	120–130 (46–53)
Osprey		150–180 (59–71)	
Bald Eagle	79–96 (31–34) [n=4]	168–244 (66–96)	46–71 (18–28) [n=5]
Harris' Hawk	43 (17) [n=1]	103–119 (41–47)	28–43 (11–17) [n=2]
Swainson's Hawk	41–58 (16–23) [n=2]	112–137 (44–54)	33–41 (13–16) [n=2]
Red-tailed Hawk	36–58 (14–23) [n=10]	107–142 (42–56)	34–56 (13.5–22) [n=9]
Ferruginous Hawk	56 (22) [n=1]	135–152 (53–60)	48 (19) [n=1]
Rough-legged Hawk		122–142 (48–56)	
Golden Eagle	79–107 (31–42) [n=10]	183–229 (72–90)	46–66 (18–26) [n=11]
American Kestrel	20–25 (8–10) [n=4]	51–61 (20–24)	15–20 (6–8) [n=4]
Merlin		53–69 (21–27)	
Peregrine Falcon	33–51 (13–20) [n=2]	94–117 (37–46)	28–38 (11–15) [n=3]
Prairie Falcon	41 (16) [n=1]	91–112 (36–44)	33 (13) [n=1]
Barn Owl	38–51 (15–20) [n=4]	104–117 (41–46)	25–38 (10–15) [n=4]
Great Horned Owl	43–64 (17–25) [n=8]	114–130 (45–51)	31–41 (12–16) [n=8]

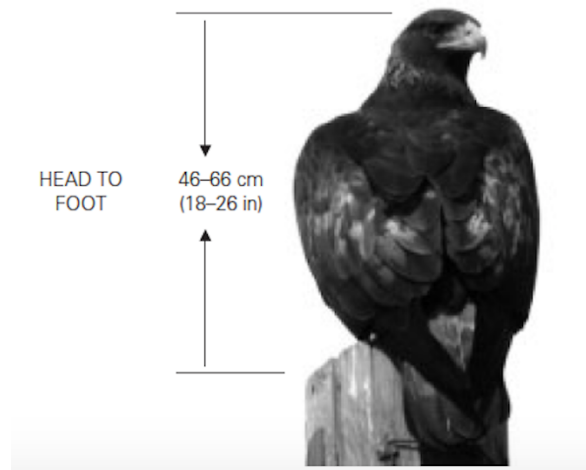
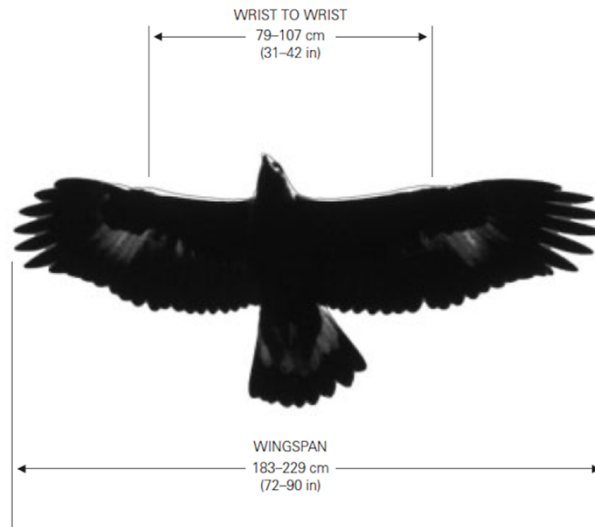


Figure 1.2.1 Critical Dimension of the Gold Eagle

1.3 Raptor Guard Description

Two fundamental concepts are supposed to be interpreted when attempting to consider avian safety: isolation and insulation. The term isolation indicates that a minimum separation between phase conductors or a phase conductor and grounded hardware is required. New or rebuilt structures with a high electrocution possibility should take this concept into consideration. The term insulation refers to covering phases or grounds where

adequate separation is not feasible. This study would provide with a deep discussion on the second concept.

One feasible insulation method is the raptor guard, a dielectric cover device separating the live being from energized devices. It is installed either on the grounded side or the conductor side. The material of the raptor guard must be physical and chemical steady, not only tolerating high voltage, but also erosion by ultraviolet rays, high environmental temperature, birds' feces, and other contamination. Aging might be a big challenge for the raptor guard and some improvements should be done according to various climate conditions, such as thick snowfall in the north and heavy humidity off the coast.

To verify the effectiveness of the raptor guard, this thesis selects the plan from Salt River Project as the research example. They came up with the hinged pole guard to insulate the raptor from the ground when they touch the high voltage side at the same time. This guard is composed of several slats according to the pole dimension. Each slat is $7.63 \times 23.65 \times 0.126$ inches and combined by SCH 80 PVC connection rings. The insulator side pole is fully covered by this guard. On the opposite side, two locking keys attached on key plates hold this guard tight on the pole.

The primary use of this device is for 69 kV poles and will be utilized on lines up to 138 kV if successful. The device has to maintain the adequate puncture strength under dry and wet conditions, should not degrade under UV radiation, and should not track under wet conditions.

This design is easy to install and adjusts to various pole diameters. In actual field work, a group of four workers can finish three guards' installations within 20 minutes. First, they apply a guard to the objective pole to estimate how many slats are necessary, then **two**

workers on the ground regulate three groups of guards based on estimation. Finally, two workers lifted by the engineering vehicle use a long bar to fix this equipment to the pole. All processes are supposed to be finished under deenergized conditions.



Figure 1.3.1 Guard's Slat Adjustment



Figure 1.3.2 Raptor Guard Installation

2 FINITE DIFFERENCE METHOD

2.1 Introduction

The Finite Difference Method (FDM) is a numerical approach used to calculate the electromagnetic field. The fundamental idea is the approximation of finite difference. FDM discretizes the partial differential equations by Taylor's theorem, replacing the partial derivative with its difference quotient, which only incorporates basic arithmetic. It is beneficial to greatly reduce the calculation complexity despite the inevitable creation of a tiny error during the replacement [7] – [8].

For most physical fields, including electromagnetic fields, the usual procedure of FDM is:

- Discretize the objective field by grid subdivision.
- Convert the partial derivative equations into the difference quotient form.
- Apply the corresponding iteration method to find the solution.

2.2 Finite Difference and Difference Quotient

As mentioned above, FDM is a mathematical method based on the difference quotient form. FDM uses the difference quotient from the discrete function value to approximate the corresponding partial derivative. Assuming a function $f(x)$, a tiny increment of $\Delta x = h$ will lead to an increase in function $f(x)$ by

$$\Delta f(x) = f(x + h) - f(x) \quad (2-1)$$

where $\Delta f(x)$ is designated as the first order difference. If the increment h is small enough, then the difference between the difference quotient Δf and the differential df is negligible.

The second order difference can be calculated by the difference quotient of first order difference, $\Delta^2 f(x)$. Similarly, we can define the high order difference quotient in this way.

For first order derivative,

$$f'(x) = \frac{df}{dx} = \lim_{\Delta x \rightarrow 0} \frac{\Delta f(x)}{\Delta x} \quad (2-2)$$

It could be approximately expressed by

$$\frac{df}{dx} \approx \frac{\Delta f(x)}{\Delta x} = \frac{f(x+h)-f(x)}{h} \quad (2-3)$$

$$\frac{df}{dx} \approx \frac{\Delta f(x)}{\Delta x} = \frac{f(x)-f(x-h)}{h} \quad (2-4)$$

or

$$\frac{df}{dx} \approx \frac{\Delta f(x)}{\Delta x} = \frac{f(x+h)-f(x-h)}{2h} \quad (2-5)$$

These three equations define the forward, backward and central difference quotient. In a geometrical plane, they represent the slope of line BC, AB and AC (Figure 2.2.1). If we expand the numerator of these equations by the Taylor polynomial, the error between the finite difference and derivative can be analyzed by:

$$f(x+h) = f(x) + hf'(x) + \frac{1}{2!}h^2f''(x) + \dots \quad (2-6)$$

$$f(x-h) = f(x) - hf'(x) + \frac{1}{2!}h^2f''(x) - \dots \quad (2-7)$$

$$f(x+h) - f(x-h) = 2hf'(x) + \frac{2}{3!}h^3f'''(x) + \dots \quad (2-8)$$

It is clear that (2-6) and (2-7) are terminated at $hf'(x)$, which means the error is directly proportional to the second order of h . However, the error of the central difference quotient is dependent on h^3 . Thus, it has the smallest termination error in approximation.

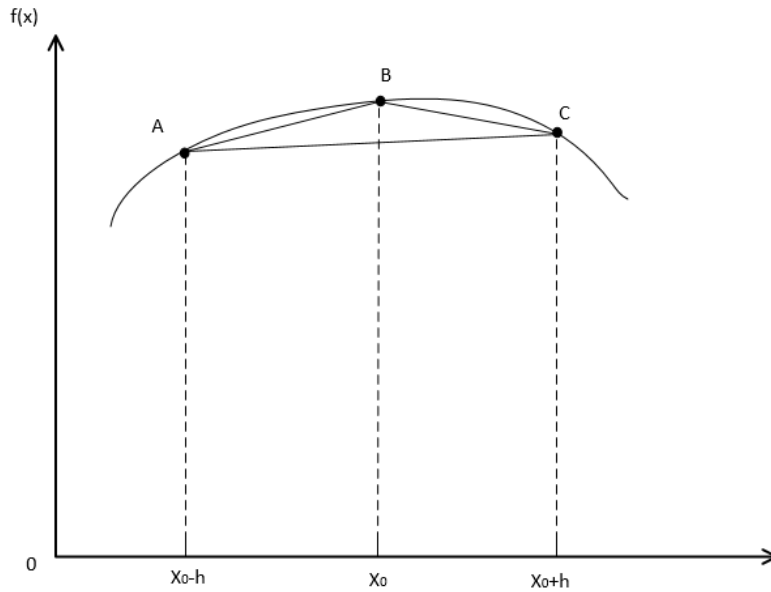


Figure 2.2.1 Point B Forward, Backward and Central Difference Quotient

Similarly, the second order difference equation can also be derived as

$$\begin{aligned} \frac{d^2f}{dx^2} &\approx \frac{1}{\Delta x} \left(\frac{df}{dx} \Big|_{x+\Delta x} - \frac{df}{dx} \Big|_x \right) \approx \frac{1}{h} \left[\frac{f(x+h) - f(x)}{h} - \frac{f(x) - f(x-h)}{h} \right] \\ &= \frac{f(x+h) - 2f(x) + f(x-h)}{h^2} \end{aligned} \quad (2-9)$$

And its Taylor polynomial is

$$f(x+h) + f(x-h) = 2f(x) + h^2 f''(x) + \frac{2}{4!} h^4 f''''(x) + \dots \quad (2-10)$$

which terminates at $h^2 f''(x)$ and the error is in the magnitude level of h^4 .

Therefore, according to equation (2-3) and (2-9), the partial differential equation can be represented by the difference quotient. For the function $u(x, y)$, if the independent variable x has a small increment $\Delta x = h$, then first order derivative in the x direction is approximately

$$\frac{\partial u}{\partial x} \approx \frac{u(x+h,y) - u(x-h,y)}{2h} \quad (2-11)$$

And second order derivative is,

$$\frac{\partial^2 u}{\partial x^2} \approx \frac{u(x+h,y) - 2u(x,y) + u(x-h,y)}{h^2} \quad (2-12)$$

2.3 Construction of the Finite Difference Format

This section adopts the two-dimensional field to explain how the Poisson equation describes the electric field. The parallel-plane electromagnetic field D , as shown in Figure 2.3.1, has a boundary defined by the closed boundary L , so that the problem could be described by Equation (2-13):

$$\begin{cases} \nabla^2 u(x, y) = \frac{\partial^2 u}{\partial x^2} + \frac{\partial^2 u}{\partial y^2} = F(x, y) & (x, y) \in D \\ u(x, y)|_L = f(r_b) \end{cases} \quad (2-13)$$

where $F(x, y)$ is the source in the field and $f(r_b)$ depicts the boundary condition of L . For the electric field without any charge in it, the source term $F(x, y) = 0$. In this case, Equation (2-13) is also called the Laplace equation.

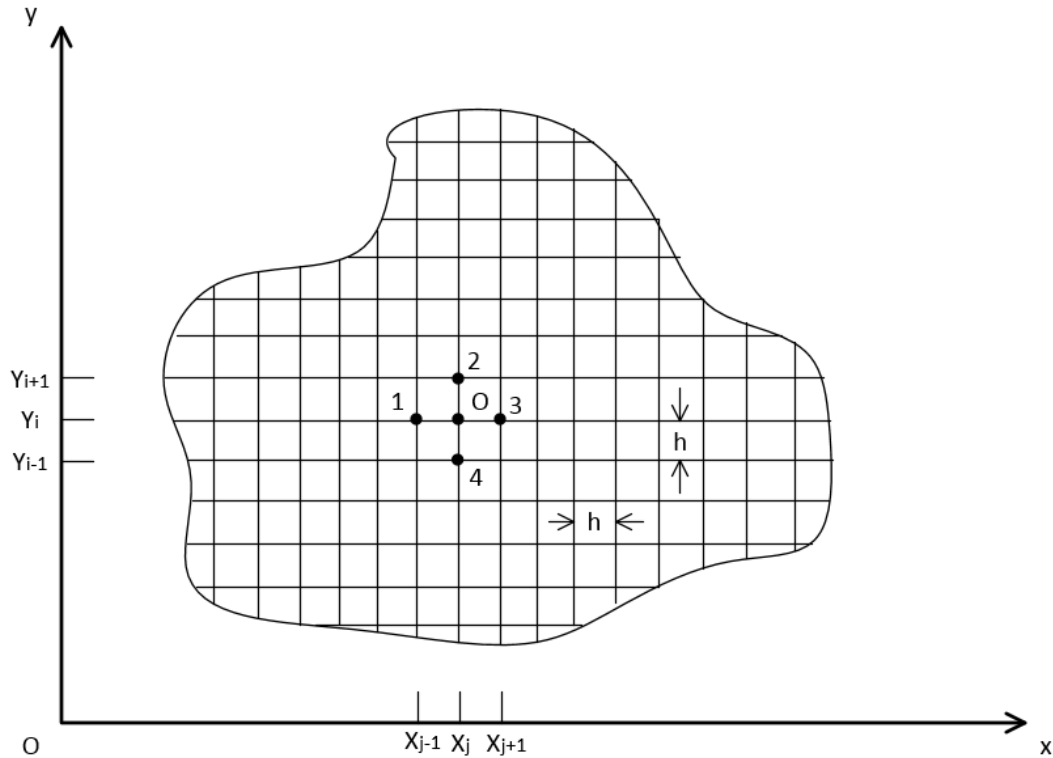


Figure 2.3.1 Objective Field Discretization by Five-points Finite Difference Method

Grid subdivision is the first step of the Finite Difference Method. The objective area is broken up into the unit of small squares, which is called the regular square arrangement, to simplify the problem. Each point acquires the difference equation in the same format, which leads to a faster solving speed. In other words, a grid that is labeled by a parallel x y coordinate, divides the objective area into small squares. The line intersection is called a “node”. In this way, the field domain D is discretized to the assembly of network nodes.

Take “node O” in Figure 2.3.1 as an example. The adjacent points 1, 2, 3 and 4 constitute a symmetrical star. The double subscript (i, j) denotes its coordinate in the horizontal and vertical axis. Each node’s potential is written as $u_0 = u_{(i,j)}$, $u_1 = u_{(i-1,j)}$,

$u_2 = u_{(i,j+1)}$, $u_3 = u_{(i+1,j)}$ and $u_4 = u_{(i,j-1)}$. According to Equation (2-9) and (2-10), the two-dimensional Poisson equation could be discretized as:

$$\frac{1}{h^2} [u_{(i+1,j)} - 2u_{(i,j)} + u_{(i-1,j)}] + \frac{1}{h^2} [u_{(i,j+1)} - 2u_{(i,j)} + u_{(i,j-1)}] = F \quad (2-14)$$

or

$$u_{(i+1,j)} + u_{(i-1,j)} + u_{(i,j+1)} + u_{(i,j-1)} - 4u_{(i,j)} = h^2F \quad (2-15)$$

Equations (2-14) and (2-15) are the difference equations of the Poisson equation. For the potential equation which meets the requirement of Laplace equation ($F=0$), its difference format is

$$u_{(i+1,j)} + u_{(i-1,j)} + u_{(i,j+1)} + u_{(i,j-1)} - 4u_{(i,j)} = 0 \quad (2-16)$$

Since the central node potential is only dependent on the adjacent four points, this method is called the five-point difference method.

2.4 Difference Format of the Boundary Condition

The setting of the boundary condition plays a vital role in the accuracy of simulation. There are various difference equation formats that are dependent on electromagnetic characteristics and the geometrical shapes of the interface. In this thesis, only two typical boundary conditions are analyzed.

2.4.1 Material Interface Overlap the Network Line

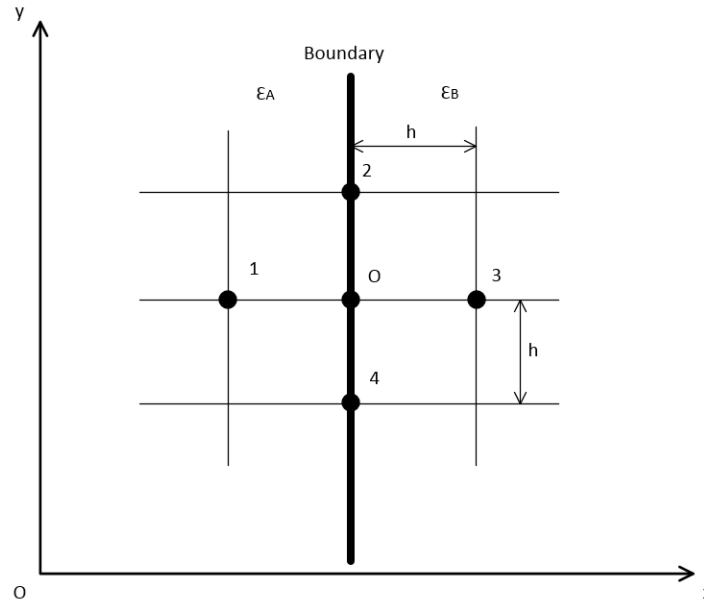


Figure 2.4.1 Material Interface Overlaps the Vertical Network Line

Suppose the interface of two materials overlap the grid line, as shown in Figure 2.1.3, node O, 2 and 4 are on the interface. The left region contains material A with permittivity ϵ_a and the right region contains material B with permittivity ϵ_b . Thus, in view of node O on the left side, the difference equation is

$$u_{a1} + u_{a2} + u_{a3} + u_{a4} - 4u_{ao} = 0 \quad (2-17)$$

While for node O on the right side, the difference equation could be written as

$$u_{b1} + u_{b2} + u_{b3} + u_{b4} - 4u_{bo} = 0 \quad (2-18)$$

However, the potential on the interface is continuous, which means:

$$u_{ai} = u_{bi} = u_i \quad (i = o, 2, 4) \quad (2-19)$$

If there is no free charge on the interface, then

$$\epsilon_a \frac{\partial u_a}{\partial n} = \epsilon_b \frac{\partial u_b}{\partial n} \quad (2-20)$$

In the difference format, it can be written as,

$$\varepsilon_a(u_{a3} - u_{a1}) \approx \varepsilon_b(u_{b3} - u_{b1}) \quad (2-21)$$

The difference equation for the node on the interface of two materials can be acquired by first multiplying Equation (2-17) and (2-18) by ε_a and ε_b , respectively, and taking their sum. Then substitute Equations (2-20) and (2-21) into the result of the previous sum.

$$u_o = \frac{1}{4} \left(\frac{2}{1+K} u_{b3} + u_2 + \frac{2K}{1+K} u_{a1} + u_4 \right) \quad (2-22)$$

where $K = \varepsilon_a / \varepsilon_b$

2.4.2 Material Interface on the Diagonal of Network

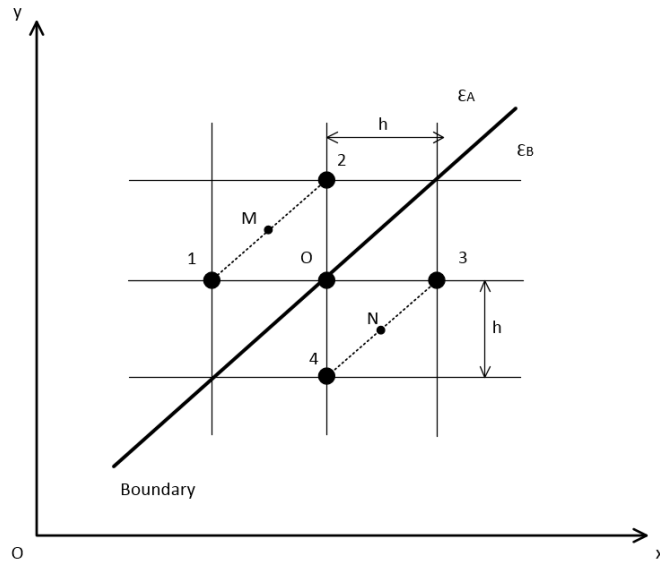


Figure 2.4.2 Material Interface Overlaps the Horizontal Grid Line

The derivation for this type of node is similar to the previous one. Nevertheless, it is necessary to introduce two auxiliary nodes M and N that are the center of lines 12 and 34 in Figure 2.1.4. If the materials A and B replace the original uniform material, the five-point difference equations are still the same as Equation (2-17) and (2-18). The interface boundary conditions are

$$u_{ao} = u_{bo} = u_o \quad (2-23)$$

$$\epsilon_a(u_{aN} - u_{aM}) \approx \epsilon_b(u_{bN} - u_{bM}) \quad (2-24)$$

where u_{aN} , u_{aM} , u_{bN} and u_{bM} are all nominal potential values which are calculated by linear interpolation.

$$2u_{aN} = u_{a3} + u_{a4} \quad (2-25)$$

$$2u_{aM} = u_{a2} + u_{a1} \quad (2-26)$$

$$2u_{bN} = u_{b3} + u_{b4} \quad (2-27)$$

$$2u_{bM} = u_{b2} + u_{b1} \quad (2-28)$$

If all these nominal values are cancelled, the difference format for this boundary condition is

$$u_o = \frac{1}{4} \left(\frac{2}{1+K} (u_{b3} + u_{b4}) + \frac{2K}{1+K} (u_{a1} + u_{a2}) \right) \quad (2-29)$$

2.4.3 Nodes at the Interface Corner

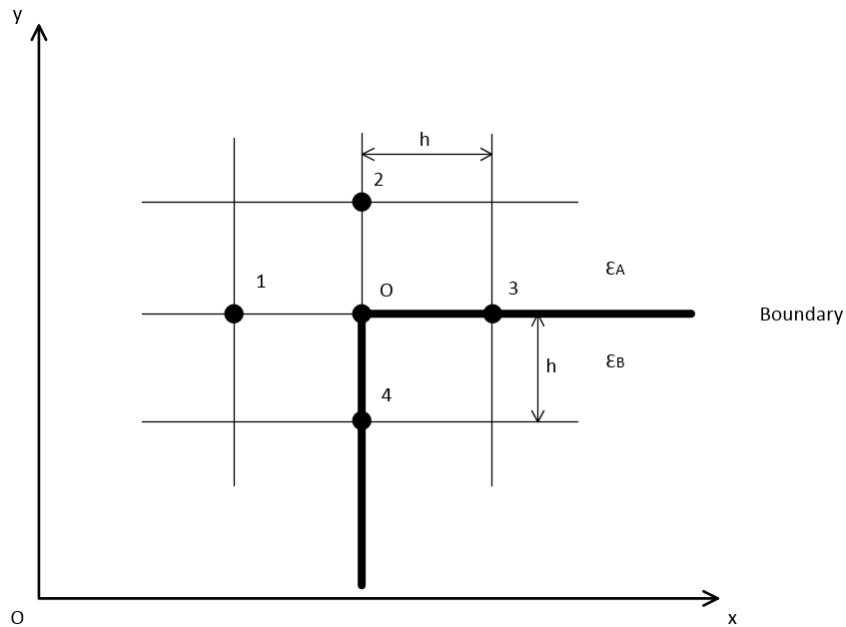


Figure 2.4.3 Node at Interface Corner

For the point lying on the boundary corner, its difference format involves more than five nodes. However, in simulation the corner nodes only account for less than 0.01% of total position, and the potential values do not deviate much. The corner point can be treated as the line boundary point to avoid this tedious work and to improve the efficiency of the code.

2.4.4 Purely Capacitive Media vs. Conductive Media

In a purely capacitive arrangement without any conducting material, the electric field could be formulated as shown in the previous section. However, once the volume resistivity is considered [8], the electric field changes to:

$$\text{div} (\epsilon E) = q \quad (2-30)$$

If J represents the current density in space,

$$J = \sigma E = \frac{E}{\rho} \quad (2-31)$$

where σ is the conductivity of the material, or in other word, the reciprocal of resistivity.

Thus,

$$\text{div} J = - \frac{\partial q}{\partial t} = \text{div} \left(\frac{E}{\rho} \right) \quad (2-32)$$

Then Equation (2-30) and (2-32) lead to,

$$\frac{\partial \text{div} (\epsilon E)}{\partial t} + \text{div} J = \frac{\partial q}{\partial t} - \frac{\partial q}{\partial t} = 0 \quad (2-33)$$

Since ϵ is independent of time, then

$$\text{div} \left(\epsilon \frac{\partial E}{\partial t} + J \right) = \text{div} \left(\epsilon \frac{\partial E}{\partial t} + \frac{E}{\rho} \right) = 0 \quad (2-34)$$

For AC fields of angular frequency ω after the Laplace transform is applied,

$$\text{div} \left(j\omega \epsilon E + \frac{E}{\rho} \right) = \text{div} \left[\left(j\omega \epsilon + \frac{1}{\rho} \right) E \right] = 0 \quad (2-35)$$

The right side of Equation (2-35) is equal to zero, which results in

$$\operatorname{div} \left[\left(\varepsilon + \frac{1}{j\omega \rho} \right) \mathbf{E} \right] = 0 \quad (2-36)$$

Therefore, the electric field including the volume resistivity can be given by replacing the permittivity in purely capacitive fields with the complex permittivity as

$$\hat{\varepsilon} = \varepsilon + \frac{1}{j\omega \rho} \quad (2-37)$$

And the boundary condition between two conductive materials can be formulated by

$$\left(\varepsilon_a + \frac{1}{j\omega \rho_a} \right) \frac{\partial u_a}{\partial n} = \left(\varepsilon_b + \frac{1}{j\omega \rho_b} \right) \frac{\partial u_b}{\partial n} \quad (2-38)$$

2.5 Solution for Difference Equation Group

For each node in the objective domain, there is a difference equation corresponding to the partial differential equation. For most nodes, the finite difference formats are the same. Thus, the iteration method is determined to be a wise option to solve this type problem.

To accelerate the rate of convergence, successive over-relaxation (SOR) is applied for most situations. As a variant of the Gauss–Seidel method for solving a linear system of equations, SOR does not use n+1th-time iteration result directly as the nth time approximate value. Instead, n+1th-time iteration result is only treated as an intermediate result for the weighted average. For example, in the five-point difference equation, the (n+1)th-time estimated value of node O should be

$$u_{(i,j)}^{(n+1)} = \frac{1}{4} \left(u_{(i+1,j)}^{(n)} + u_{(i,j+1)}^{(n)} + u_{(i-1,j)}^{(n)} + u_{(i,j-1)}^{(n)} - h^2 F \right) \quad (2-39)$$

Nevertheless, SOR may calculate it by

$$\begin{aligned} u_{(i,j)}^{(n+1)} &= u_{(i,j)}^{(n)} + \omega R_{(i,j)}^n = u_{(i,j)}^{(n)} + \omega (\bar{u}_{(i,j)}^{(n)} - u_{(i,j)}^{(n)}) \\ &= u_{(i,j)}^{(n)} + \frac{\omega}{4} (u_{(i+1,j)}^{(n)} + u_{(i,j+1)}^{(n)} + u_{(i-1,j)}^{(n)} + u_{(i,j-1)}^{(n)} - h^2 F - 4u_{(i,j)}^{(n)}) \end{aligned} \quad (2-40)$$

where ω is the relaxation factor ranging from 1 to 2. If $\omega = 1$, then Equation (2-40) converts to the original Gauss-Seidel iteration method; if $\omega \geq 2$, the result is expected to diverge instead of converge. In a rectangular field, where the length of side is “ph” and “qh” (usually p and q are greater than 15) is divided into squares with sides of length “h”, the optimum relaxation factor would be

$$\omega_{\text{opt}} = 2 - \pi\sqrt{2} \sqrt{\frac{1}{p^2} + \frac{1}{q^2}} \quad (2-41)$$

In SOR, it is also necessary to examine the extent of convergence. The conventional method is to compare the error between two adjacent iteration results with the assigned error. If the biggest error, which is the biggest difference between the nodes matrix over two times the iteration, is not greater than the assigned error, the iteration meets the requirement of convergence.

2.6 Simulation Flow Chart

Figure 2.4.1 elaborate the process of the whole simulation.

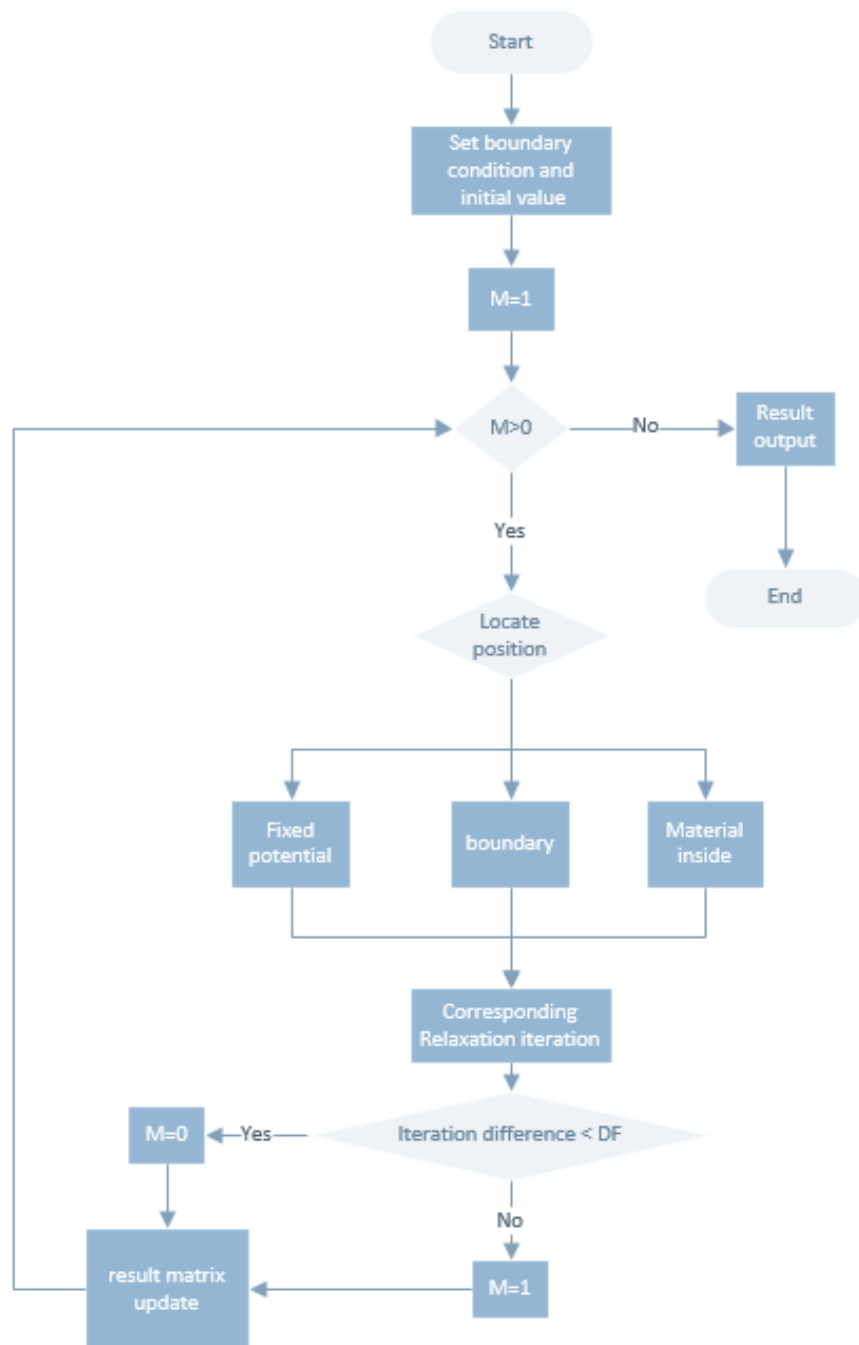


Figure 2.6.1 FDM Code Flow Chart in MATLAB

At the beginning, parameters for each part are set in the objective domain, including the initial potential, permittivity, conductivity, iteration mark M (initial value is 1), objective error and relaxation factor. Then, the system enters into the iteration cycle.

The whole cycle can be divided into two parts: matrix scan and error iteration.

a. Matrix Scan

The potential is calculated based on the mathematical model developed above. Each point will be labeled by 2-dimensional coordinates to describe its position. The node type should be identified, such as nodes on the interface, fixed-potential nodes or nodes within a domain, etc. Once the node type is clear, the system will apply the corresponding equation to acquire a new transient potential based on the last potential result, and then move on.

The code is set to scan the matrix column by column from top left to bottom right.

b. Error Iteration

Once all the nodes in the domain are scanned, the maximum difference between the current potential and the last potential, which is denoted as the "error", is acquired by matrix subtraction. If this error is greater than the objective error, then M remains at one. The matrix enters into another round of scanning until the error is smaller than the objective error. The iteration will stop when the potential matrix has no more change greater than the objective error between the two matrix scans (set $M = 0$). At this moment, the potential in the matrix would be the final potential distribution in the domain.

Since the electric field is a gradient of potential, it is easier to get this value by using the equation below:

$$E = \frac{dU}{dx} \tag{2-42}$$

Once the potential matrix is acquired, the electric field is also accessible.

3 RAPTOR-INSULATOR MODEL SIMULATION

3.1 FDM Code Validation

Prior to the raptor-guard simulation, it is critical to test the mathematical model and the algorithm. Some existing cases, where the potential and the electric field distribution have been analyzed before, should be adopted for comparison with the proposed method's results. If no obvious error exists, then its effectiveness will be proved.

The electric field in a capacitor is uniform in the majority of the area where the distance between two polar plates gets close enough. The electric field is independent of position in this case. Nevertheless, with the increase of plate's relative distance, the electric field is distorted and becomes more and more nonlinear, dropping drastically from the high-voltage plate and becoming flat when approaching the low-voltage side [9].

3.1.1 Capacitor Model with Different Length between Two Plates

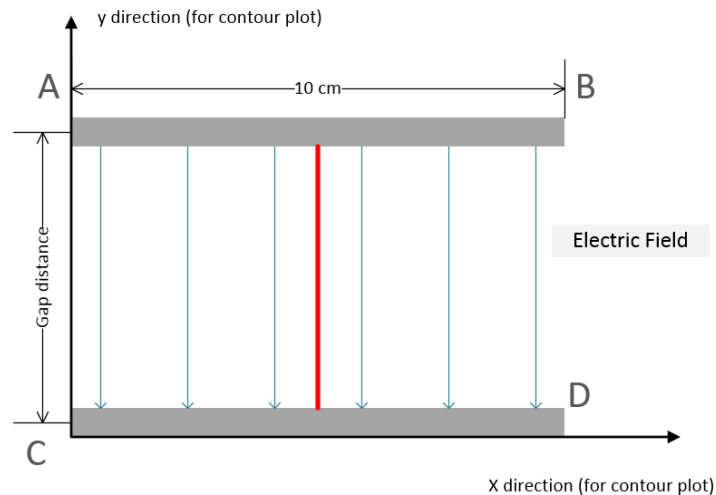


Figure 3.1.1 Simple Capacitor Model with Adjustable Plate Distance

In this section, a parallel-plate capacitor model will be examined to exhibit how the distance between plates affect the electric field distribution.

Figure 3.1.1 describe a capacitor with plate's gap d . The upper plate is energized by 40 V, and the lower plate is well grounded. The length of each plate is 5 cm. Four cases with 3 cm, 5 cm, 10 cm and 20 cm in vertical distance are compared in the following.

Since there is no electrical charge between two plates, Laplace equation plus first boundary condition are capable of picturing the potential and the electric field here.

$$\frac{\partial^2 \varphi}{\partial x^2} + \frac{\partial^2 \varphi}{\partial y^2} = 0, \quad (x, y) \in D \quad (3-1)$$

$$\varphi_{CD} = \varphi_{AC} = \varphi_{BD} = 0 \text{ V} \quad (3-2)$$

$$\varphi_{AB} = 40 \text{ V} \quad (3-3)$$

Even though the potential at the side of the capacitor (line AC and BD in Figure 3.1.1) is not zero in reality, its value is complicated to calculate in most situation. one thing for sure is that the potential drops drastically to zero outside the capacitor. Therefore, the simulation assumes a fictitious boundary at the side to represent the zero potential reference, and then calculate the vertical-direction potential at the center of the capacitor (red line in Figure 3.1.1). That is the reason why Equation (3-2) sets $\varphi_{AC} = \varphi_{BD} = 0 \text{ V}$.

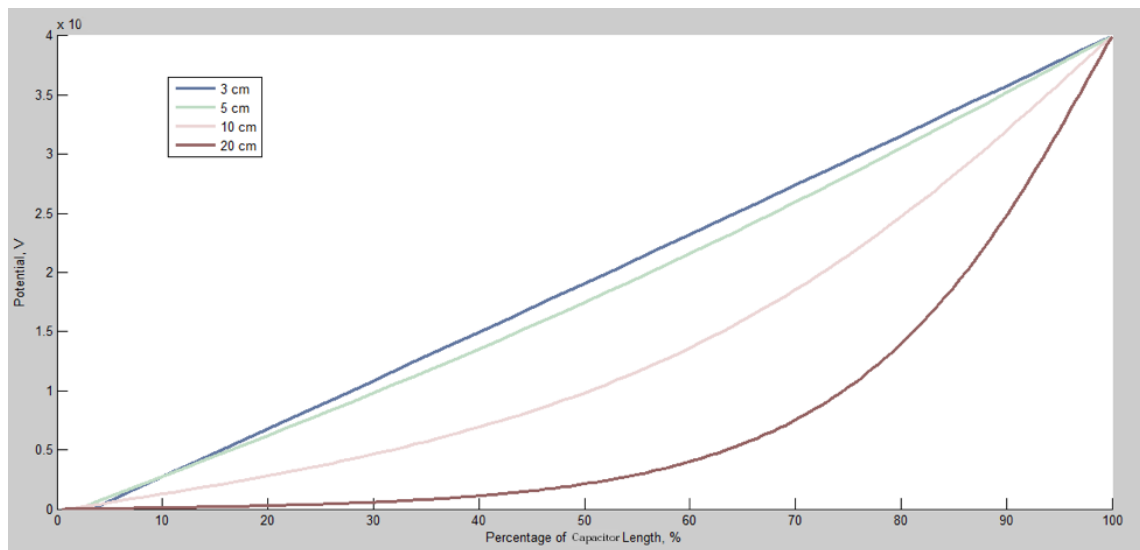


Figure 3.1.2 Potential Distribution in Vertical Direction with Various Gap Distance

The potential arrangements in the center of the capacitor model (red line position in Figure 3.1.1) are plotted in Figure 3.1.2. The horizontal axis represents the distance to the bottom plate in terms of percentage. 100% depicts the potential at the upper plate where potential is 40 V. The vertical axis indicates the potential of the corresponding position. The legend in the upper left explains which color stands for which gap distance.

It is clear that in the 3 cm case, the potential behaves in the manner of linearity, since the capacitor edge, where potential is more close to zero, has little influence on it. It could be also explained in another way: according to Equation (3-1), the horizontal component (x axis) is relatively “steady”. The zero potential boundary on the edge AC and BD is far away from the objective area compared with the influence of AB and CD. Thus we could simplify Equation (3-1) into one dimension.

$$\frac{\partial^2 \varphi}{\partial y^2} = 0, \quad (x, y) \in D \quad (3-4)$$

The second order derivative is zero, meaning its first order derivative is a constant and the original function is linear dependent on the position. This result is accordance with the simulation result for the small gap situation.

With gap distance increasing, however, the edge boundary AC and BD play a more and more vital role on the center potential distribution. In other words, $\frac{\partial^2 \varphi}{\partial x^2}$ weight is amplified because 10 cm plate length is not long enough to neglect the edge’s effect in comparison with 10 or 20 cm gap distance. Thus, the potential reduces at a great rate from the energized plate and flattens at the end. The longer the gap distance is, the more observable this phenomenon is. Figure 3.1.2 depicted 10 and 20 cm cases, too.

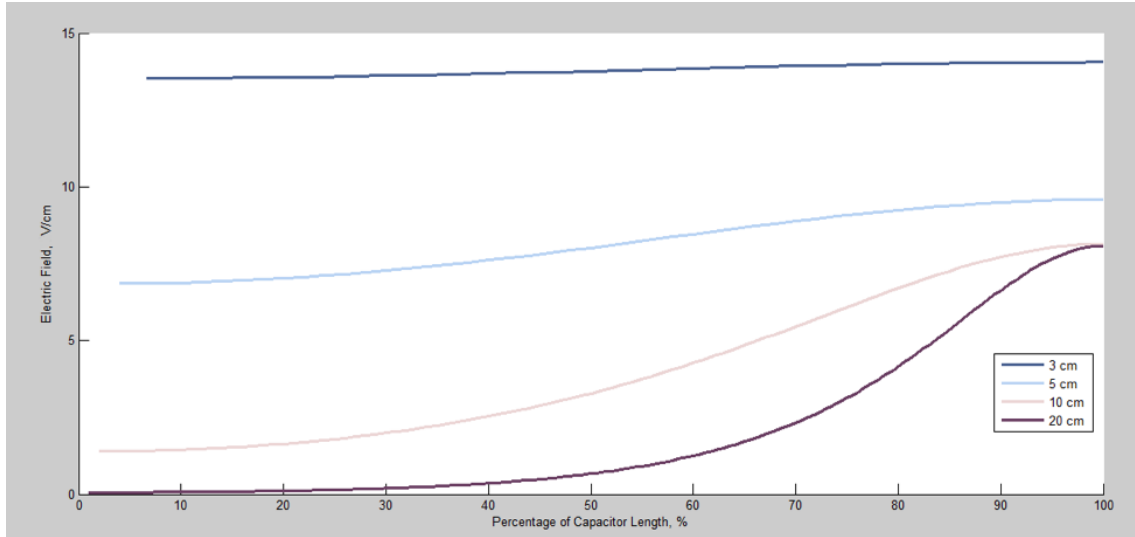


Figure 3.1.3 Electric Field in Vertical Direction with Various Gap Distance

It is not difficult to get the electric field by taking derivative of the potential. Figure 3.1.3 elaborates the electric field change for various gap distances. At the 3 cm case, the curve is a straight line, meaning the electric field is uniform and independent of position. When the gap raises up to 5 cm, 10 cm and 20 cm, nonlinearity performs more evidently, particularly in the upper half part of the capacitor. As for the reason why EF starting points lie different location at 100% length, it is because the potential of upper plate is always 40 V, whereas the average electric field decrease according to Equation (3-5)

$$EF = \frac{\text{Potential}}{\text{distance}} \quad (3-5)$$

The contour plots in Figure 3.1.4 and 3.1.5 explore more details on potential distribution. The vertical and the horizontal axis label the physical coordinates in y and x direction in Figure 3.1.1. For example, point A locates at the top left corner and point B at the top right corner. Curve close to red means high potential, whereas deeper blue represent much lower potential near zero. All potential curves converge at top corner because the

potential of the side fictitious boundary is assumed to be zero. Attention should be paid to the center of the horizontal axis.

When two plates are only 3 cm apart, the potential curves are separated roughly at the same interval. Once the gap goes up to 10 cm, the upper part curve becomes denser, indicating the potential drops quicker in the vicinity of energized plate. All these results are consistent with previous theory analysis.

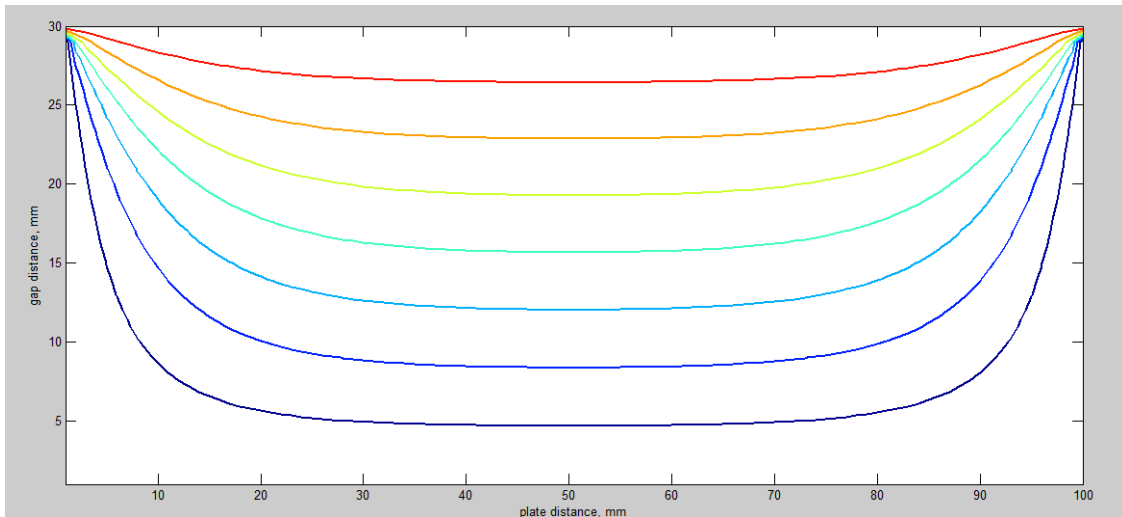


Figure 3.1.4 Potential Contour for Gap= 3 cm

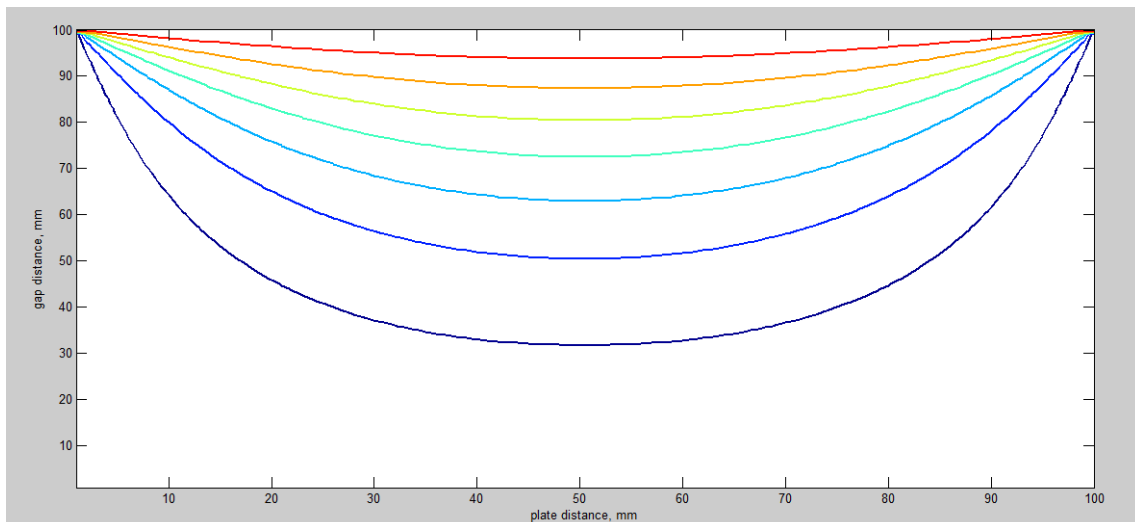


Figure 3.1.5 Potential Contour for Gap = 10 cm

3.1.2 Capacitor Model Inserted by Two Different Material

Another verification is based on a capacitor model doped by two kinds of material in Figure 3.1.6. Material A and B are divided by the diagonal line. Suppose the capacitor is a 15 cm * 15 cm square, the potential arrangement is described in Figure 3.1.7. The upper plate is energized by 10V, and the lower plate is well grounded. The vertical and horizontal axis represent the physical position of Figure 3.1.6. The legend bar at the right side mark the potential with various color.

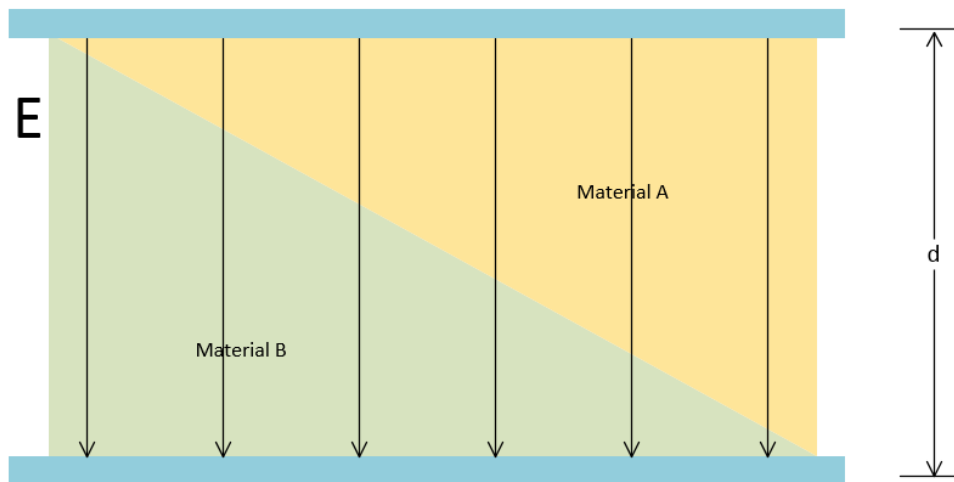


Figure 3.1.6 Two Materials Inserted into A Capacitor

It could be observed that the potential still drops from the top. However, the presence of interface distorts its flat line distribution compared with Figure 3.1.4. This result could also be interpreted in matrix form in Table 3.1 [7].

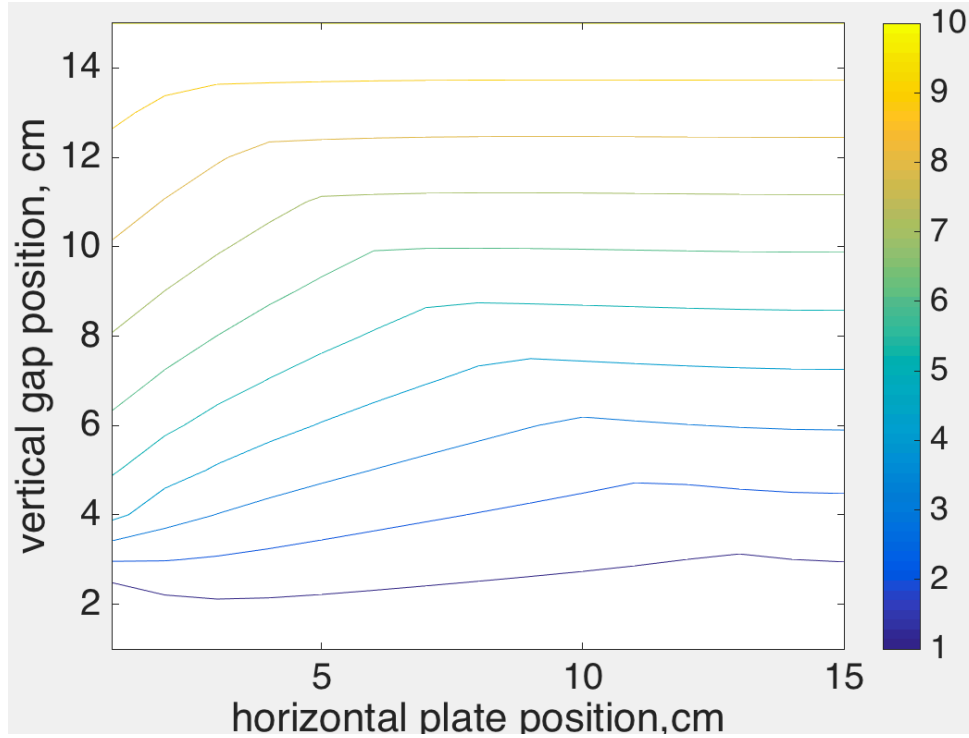


Figure 3.1.7 Potential Contour

Table 3.1 Potential Matrix Corresponding to Figure 3.1.6

15x15 double															
	1	2	3	4	5	6	7	8	9	10	11	12	13	14	15
1	10	10	10	10	10	10	10	10	10	10	10	10	10	10	10
2	9.2162	9.2159	9.2151	9.2140	9.2129	9.2122	9.2125	9.2143	9.2183	9.2253	9.2359	9.2499	9.2648	9.2698	9.4165
3	8.4329	8.4323	8.4306	8.4281	8.4255	8.4235	8.4234	8.4263	8.4337	8.4472	8.4684	8.4988	8.5396	8.8364	9.1264
4	7.6509	7.6499	7.6468	7.6423	7.6373	7.6331	7.6313	7.6338	7.6430	7.6614	7.6918	7.7375	8.0695	8.4099	8.7681
5	6.8712	6.8694	6.8645	6.8571	6.8485	6.8403	6.8349	6.8348	6.8431	6.8635	6.9000	7.2368	7.5909	7.9657	8.3669
6	6.0949	6.0923	6.0847	6.0731	6.0591	6.0449	6.0332	6.0274	6.0313	6.0496	6.3723	6.7187	7.0919	7.4950	7.9309
7	5.3240	5.3201	5.3089	5.2915	5.2700	5.2470	5.2257	5.2102	5.2051	5.4997	5.8211	6.1739	6.5629	6.9917	7.4613
8	4.5609	4.5553	4.5392	4.5141	4.4825	4.4473	4.4126	4.3826	4.6398	4.9231	5.2384	5.5930	5.9941	6.4478	6.9545
9	3.8089	3.8012	3.7786	3.7434	3.6984	3.6474	3.5945	3.8105	4.0484	4.3144	4.6166	4.9654	5.3729	5.8508	6.4026
10	3.0725	3.0618	3.0307	2.9823	2.9204	2.8492	3.0249	3.2163	3.4288	3.6696	3.9483	4.2791	4.6815	5.1798	5.7911
11	2.3576	2.3427	2.3002	2.2348	2.1515	2.2912	2.4396	2.6011	2.7811	2.9867	3.2280	3.5212	3.8941	4.3959	5.0935
12	1.6726	1.6513	1.5927	1.5050	1.6141	1.7247	1.8410	1.9672	2.1079	2.2682	2.4559	2.6834	2.9779	3.4162	4.2548
13	1.0302	0.9971	0.9144	0.9978	1.0754	1.1524	1.2325	1.3191	1.4148	1.5225	1.6440	1.7786	1.9179	2.0362	2.0818
14	0.4538	0.3926	0.4509	0.4965	0.5372	0.5768	0.6178	0.6617	0.7098	0.7628	0.8190	0.8691	0.8790	0.7288	0
15	0	0	0	0	0	0	0	0	0	0	0	0	0	0	0

3.2 Insulator Model ----Shed Model vs. Bar Model

Most insulators, either composed of porcelain or polymer, have the shed structure to maximize creepage distance. These gaps between sheds provide a longer pathway for the ionized particle. It also warps the nearby electric field. To develop an accurate model, the shed structure ought to be adopted in the potential and the electric field computations.

However, the coding complexity of the finite difference method is mainly dependent on how many boundary conditions there are. The protruding part of each shed, even though they repeat at a constant interval, are bound to increase the codes' complexity and make the computation less efficient.

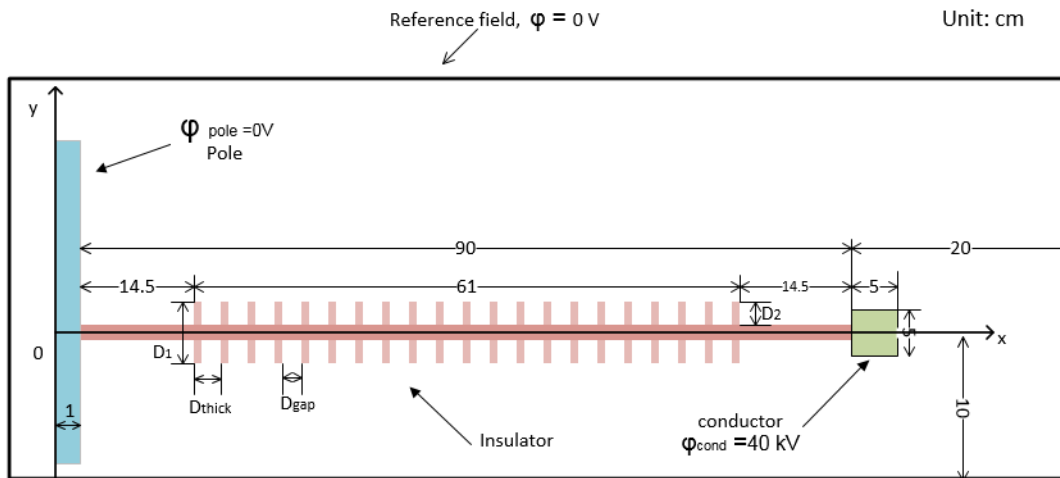


Figure 3.2.1 Shed Insulator Model Example in 69 kV System

To verify how much effect these shed gaps have on the electric field, it is necessary to compare two types of models: the shed model and the bar model. The former one incorporates protuberance of the shed as shown in Figure 3.2.1. The blue part on the left side represents the metal pole, the green square on the right side is the conductor, and insulator is depicted with pink color, which connects the pole and the conductor. The white

area within the black boundary represents air. The reference field where potential $\phi = 0V$ is the environmental zero point which has been discussed in Chapter #3. Detailed dimension parameters are described in Table 3.2 and Figure 3.2.1.

Table 3.2 Shed Insulator Model Parameters

Total length, mm	Length of whole shed, mm	Number of shed, mm	Gap between sheds D_{gap} , mm	Thickness of shed D_{thick} , mm	Total diameter $D1$, mm	Bar diameter, mm	Protrude distance $D2$, mm
900	630	21	20	10	76	24	26

Based on the model above, if we assume the phase-to-ground voltage of the conductor is 40 kV and the pole is well-grounded (always zero in voltage), the potential and electric field on the insulator surface are shown in Figure 3.2.2 and Figure 3.2.3.

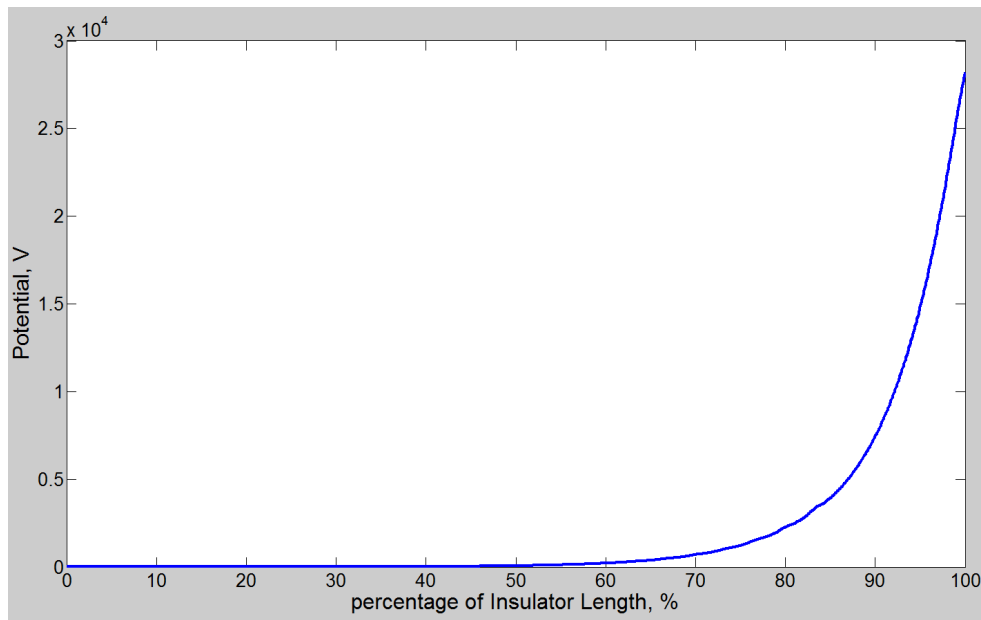


Figure 3.2.2 Potential along Shed Insulator

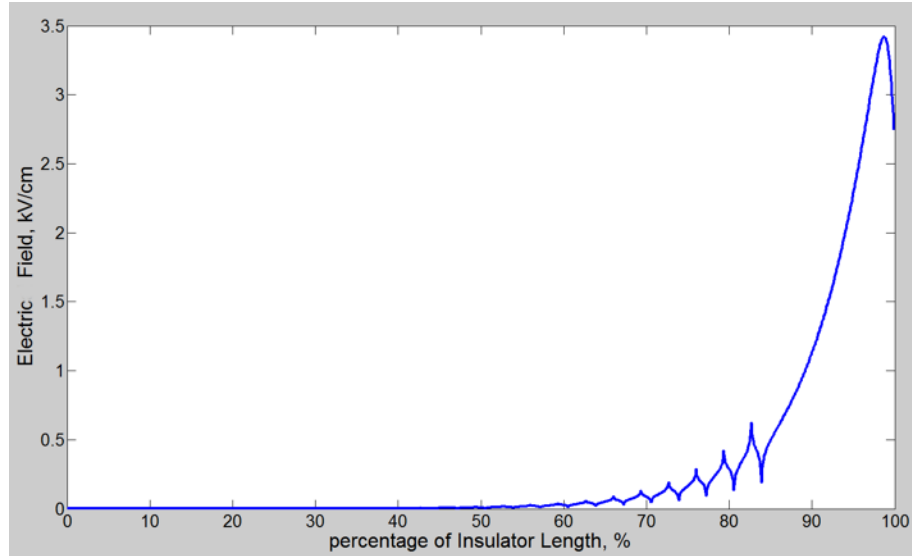


Figure 3.2.3 Electric Field along Shed Insulator

Figure 3.2.3 indicates that the shed configuration results in the fluctuating line of the electric field, but the tendency is downward from the conductor side (100% length) to the ground side (0% length).

To reduce the simulation time and the model complexity, the bar model, which remove the variables of protrusion, is applied in the following.

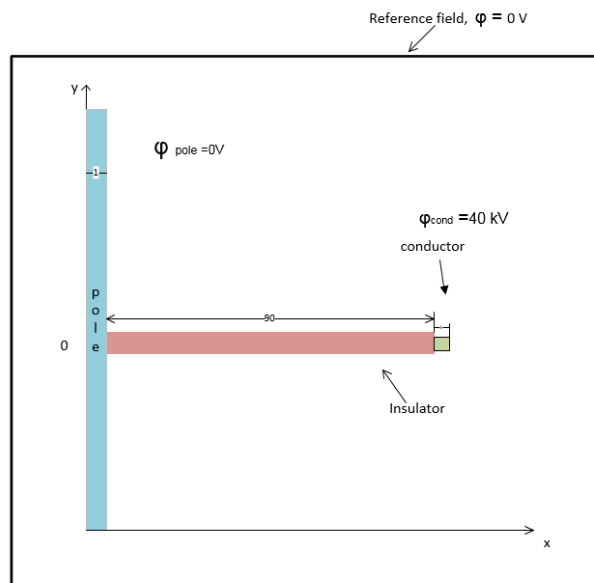


Figure 3.2.4 Bar Insulator Model Example in 69 kV System

To make it comparable, each component in the objective area keeps the same dimension, except the shed insulator is replaced by a 90×5 cm straight bar insulator. Due to the smooth surface, the lines of code is 75% less than the previous situation. If the parameters are still same, the simulation results are shown below.

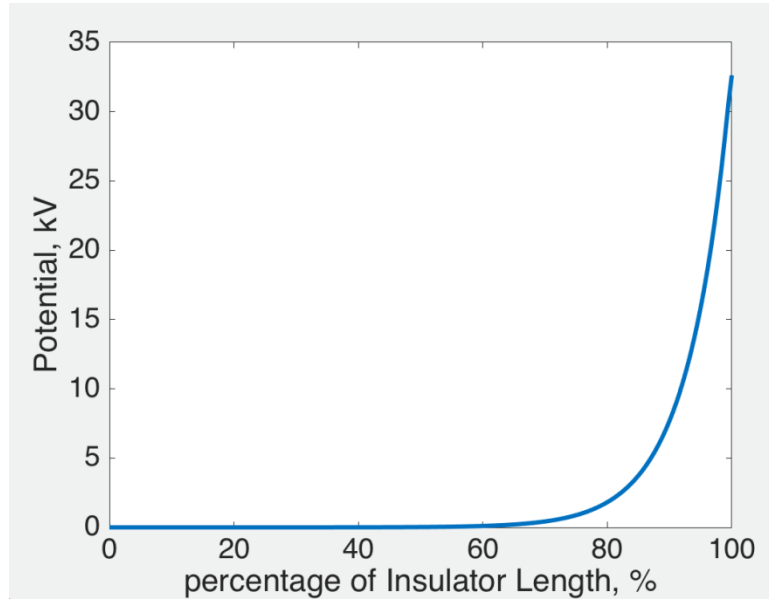


Figure 3.2.5 Potential along Bar Insulator

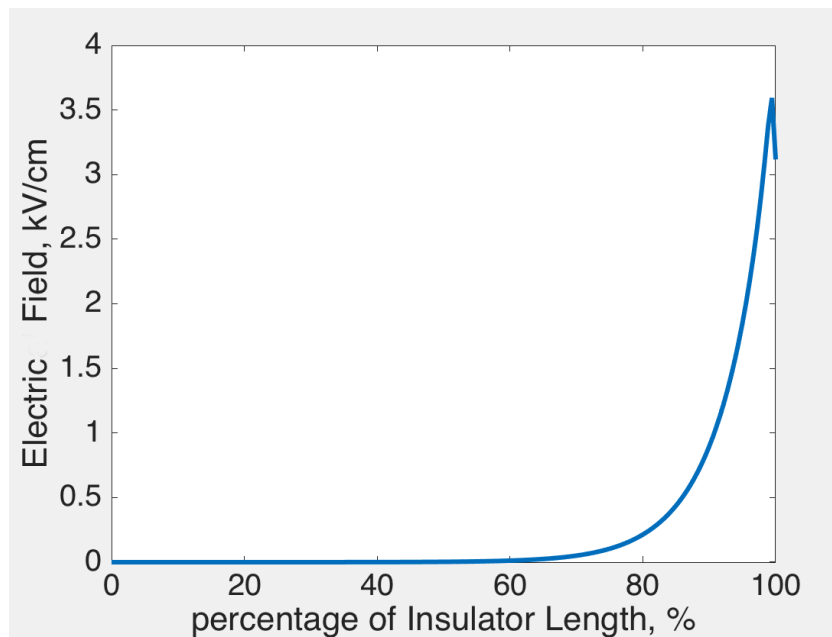


Figure 3.2.6 Electric Field along Bar Insulator

The potential distribution in Figure 3.2.5 is quite similar to that in the shed model, cascading rapidly from the right side. The electric field experiences the same trend as the one in the shed model, too. The only difference is a small fluctuation at the end of the shed structure near the conductor side. However, the shed radius is relatively short compared with the total length of the insulator, so that the distortion of electric field by the shed structure does not play an influential role from the overall perspective.

The key point is that in the massive model which includes so many intricate boundaries, code lines may increase drastically [9]. One square protrusion on a flat surface will add three additional line-boundary conditions and four additional corner-boundary conditions. More complicated contact for various material, such as zigzag or randomized interface, will give rise to huge code quantity. Therefore, in consideration of less impact on the electric field, the bar insulator model will be applied in the following simulation.

3.3 Raptor-Insulator Model

The red tail hawk is the primary raptor electrocuted in Arizona State according to the SRP report. In Chapter #1, the height, wingspan and wrist-to-wrist measurements of the red tail hawk are 34 to 56 cm, 107 to 142 cm and 36 to 58 cm respectively. In consideration of the simulating commonality, the raptor dimension in the simulation is 35 cm in height, 48 cm in wrist-to-wrist and 82 cm in wingspan. One noticeable thing is that the wingspan in the simulation is not the spreading wingspan in common sense, wings are folded downward to simulate the electrocution where the raptor touch the conductor and pole at the same time. The usual posture of electrocution is the stance before taking off. At that moment, raptor's wings expand askew from its body. But the boundary condition setting

would be much more intricate if the boundary is not in parallel with any gird line. So that the raptor is assumed to bend its wings at 90 degrees for simulating feasibility at the cost of accuracy.

Furthermore, the horizontal trunnion line post insulator is the main type installed in the objective area. Figure 3.3.1 introduces the specific dimension marked by yellow color [11].

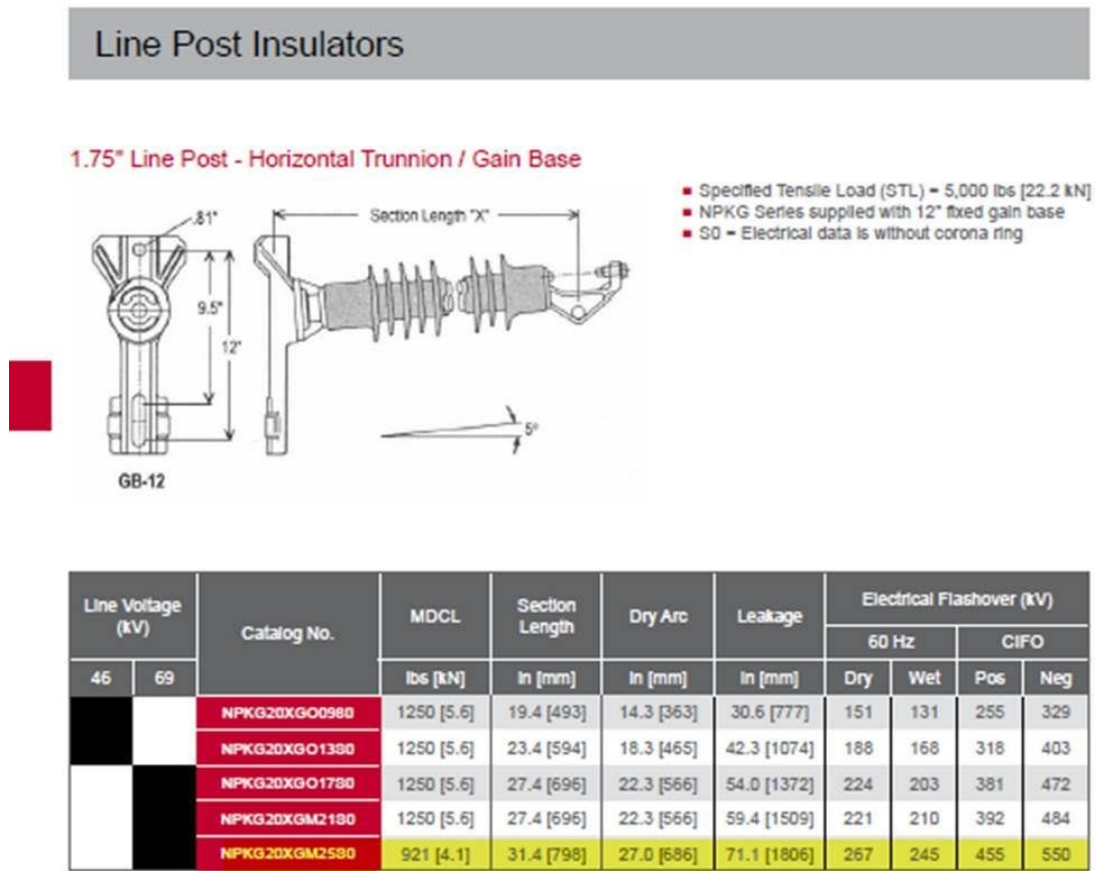


Figure 3.3.1 Line Post Insulator Parameter

954ACSS O.D. Bare Conductor with 1.165 inches (2.959 cm) is selected in the conductor simulation of 69 kV system.

Raptor guard's height is 23.75 inches (60.325 cm), and the thickness is 0.126 inches (0.32 cm).

According to the data listed above, the simulation model is illustrated in Figure 3.3.2.

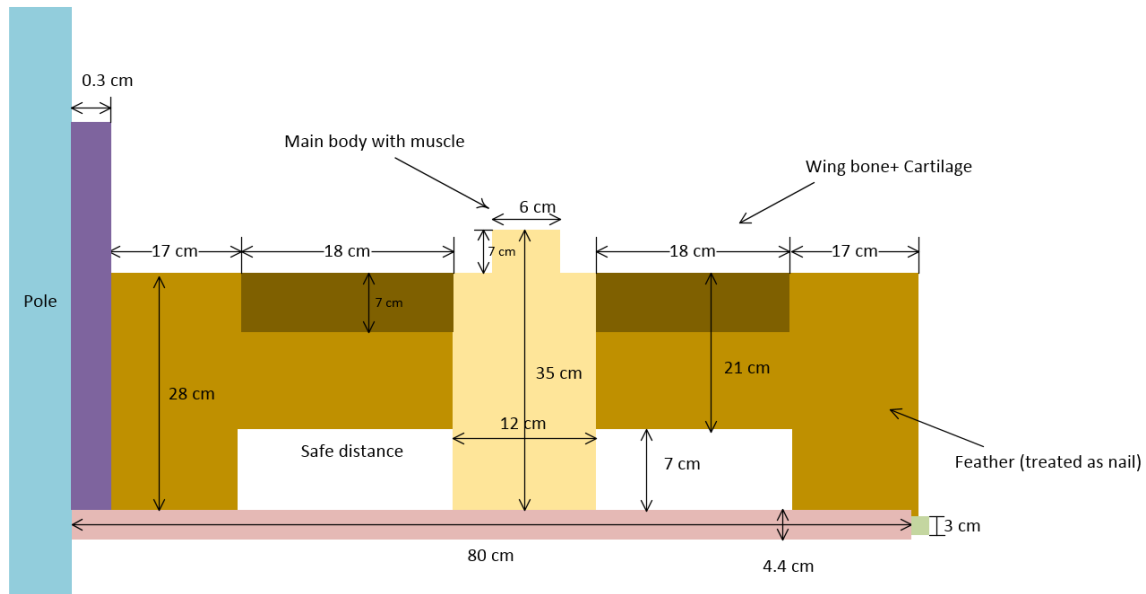


Figure 3.3.2 Raptor Model Diagram with Detailed Dimension

3.4 Parameter Setting

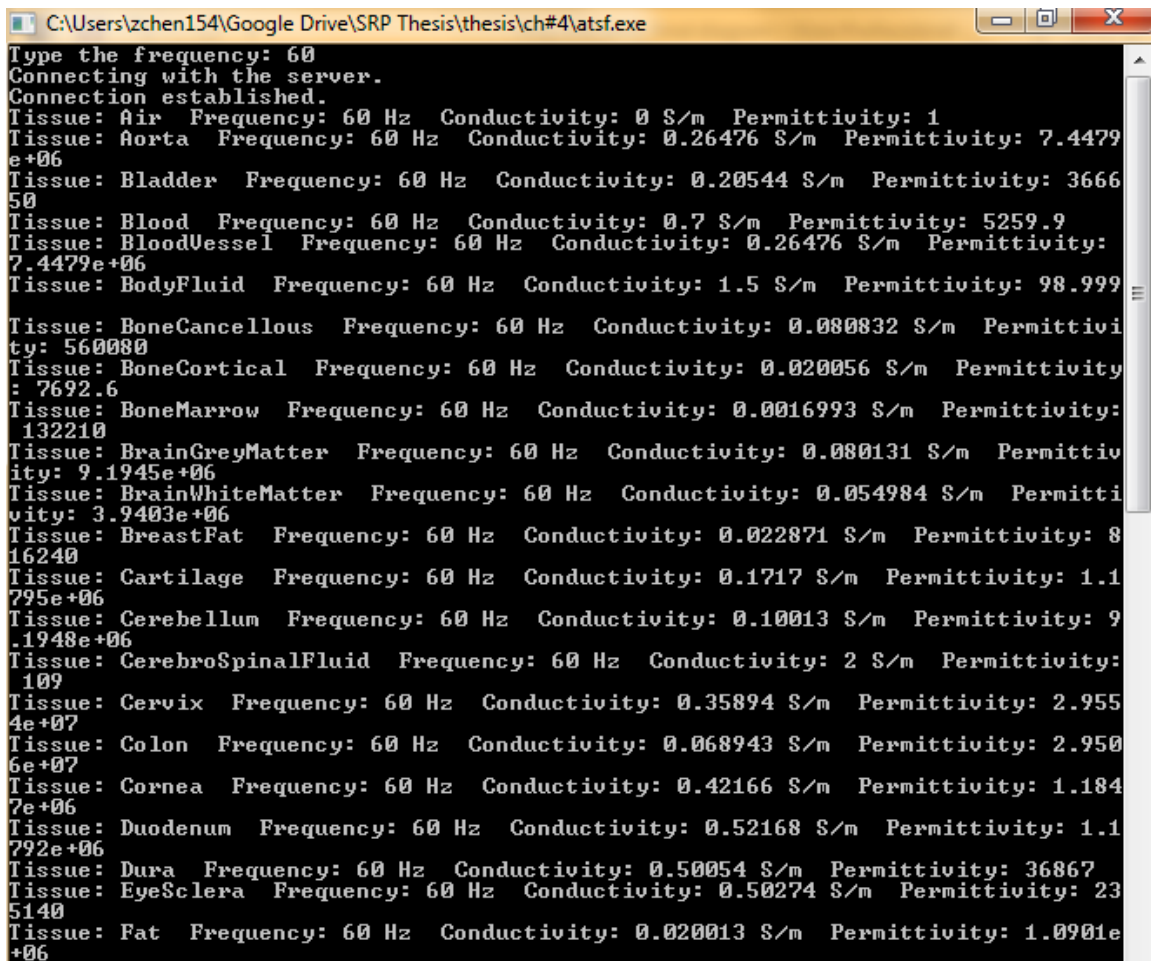
Bio-impedance is a complicated topic since either humans or animals are constituted of various organs with different electric properties. It is not hard to find the data for a single tissue, but the modeling of a whole body seems impossible only by the simple combination of organs. Most data and models of the bio-impedance originate from the experimental measurement. No applicable raptor bio-impedance model has been found so far.

Another obstacle for the raptor model would be the raptor tissue data. Even though there is plenty of research on the human body, only a few papers discussed quantitatively birds or raptors in the past decades.

Since no experiment on the live raptor or dead body is permitted, an analogy between humans and red tail hawks is made. The raptor body is divided into three parts: the main body with muscle, the wing bone plus cartilage and the feather according to its

physiological structure. Each part corresponds to a human organ whose electrical parameter is known.

Fortunately, the Italian national research council published a server program which includes dielectric properties of human body tissues under various power frequency [12]. After typing in the objective frequency, conductivity and permittivity data is exhibited in this exe file. (Figure 3.4.1).



```
C:\Users\zchen154\Google Drive\SRP Thesis\thesis\ch#4\atsf.exe
Type the frequency: 60
Connecting with the server.
Connection established.
Tissue: Air Frequency: 60 Hz Conductivity: 0 S/m Permittivity: 1
Tissue: Aorta Frequency: 60 Hz Conductivity: 0.26476 S/m Permittivity: 7.4479
e+06
Tissue: Bladder Frequency: 60 Hz Conductivity: 0.20544 S/m Permittivity: 3666
50
Tissue: Blood Frequency: 60 Hz Conductivity: 0.7 S/m Permittivity: 5259.9
Tissue: BloodVessel Frequency: 60 Hz Conductivity: 0.26476 S/m Permittivity:
7.4479e+06
Tissue: BodyFluid Frequency: 60 Hz Conductivity: 1.5 S/m Permittivity: 98.999
Tissue: BoneCancellous Frequency: 60 Hz Conductivity: 0.080832 S/m Permittivi
ty: 560080
Tissue: BoneCortical Frequency: 60 Hz Conductivity: 0.020056 S/m Permittivity
: 7692.6
Tissue: BoneMarrow Frequency: 60 Hz Conductivity: 0.0016993 S/m Permittivity:
132210
Tissue: BrainGreyMatter Frequency: 60 Hz Conductivity: 0.080131 S/m Permittiv
ity: 9.1945e+06
Tissue: BrainWhiteMatter Frequency: 60 Hz Conductivity: 0.054984 S/m Permitti
vity: 3.9403e+06
Tissue: BreastFat Frequency: 60 Hz Conductivity: 0.022871 S/m Permittivity: 8
16240
Tissue: Cartilage Frequency: 60 Hz Conductivity: 0.1717 S/m Permittivity: 1.1
795e+06
Tissue: Cerebellum Frequency: 60 Hz Conductivity: 0.10013 S/m Permittivity: 9
.1948e+06
Tissue: CerebroSpinalFluid Frequency: 60 Hz Conductivity: 2 S/m Permittivity:
109
Tissue: Cervix Frequency: 60 Hz Conductivity: 0.35894 S/m Permittivity: 2.955
4e+07
Tissue: Colon Frequency: 60 Hz Conductivity: 0.068943 S/m Permittivity: 2.950
6e+07
Tissue: Cornea Frequency: 60 Hz Conductivity: 0.42166 S/m Permittivity: 1.184
7e+06
Tissue: Duodenum Frequency: 60 Hz Conductivity: 0.52168 S/m Permittivity: 1.1
792e+06
Tissue: Dura Frequency: 60 Hz Conductivity: 0.50054 S/m Permittivity: 36867
Tissue: EyeSclera Frequency: 60 Hz Conductivity: 0.50274 S/m Permittivity: 23
5140
Tissue: Fat Frequency: 60 Hz Conductivity: 0.020013 S/m Permittivity: 1.0901e
+06
```

Figure 3.4.1 Human Bio-Impedance under 60 Hz

Therefore, muscle and bone cortical in Figure 3.4.1 are selected to match the first two parts of raptor. Humans, nevertheless, do not have a similar apparatus like the feather. In

1980, Morlan W. Nelson did several experiments on the golden eagle under the sponsorship of Idaho Power Company (details in Chapter #4). It was shown that the feather may tolerate voltage over 70 kV, much higher than the limit of the flesh like toes. So the feathers may appear like dielectric materials and set conductivity and permittivity with 5×10^{-3} S/m and 2×10^3 , respectively. Table 4.2 summarizes all electrical properties used in the subsequent simulation.

Table 3.3 Raptor Model Parameter Setting

Raptor Tissue	Human Body Analogy	Conductivity S/m	Relative Permittivity
Main Body with Muscle	Muscle	2.42E-01	1.56E+07
Bone + Cartilage	Bone Cortical	2.01E-02	7.69E+03
Feather	None	5.00E-03	2.00E+03
Air		5.00E-15	1
Raptor Guard Polyethylene		1.00E-13	6
Insulator		1.00E-13	4

Because there are 6 types of materials with diverse natures and also two first-boundary conditions for pole and conductor, categorization of the interface becomes significant. Figure 3.4.2 and 3.4.3 elaborate the identification number for each boundary. These red numbers are helpful in coding in case confusing or omitting any boundary condition.

As mentioned in Chapter #2, corner points are classified into the line boundary points for the model simplification. In Figure 3.4.2, three types of corner points are labeled with different colors, representing different setting methods. Red points are deemed as a starting point of the horizontal line at its right side; for instance, the point, whose coordinates is (17.4, 68), is the starting point for boundary #9. Green points and blue points stand for points belonging to the vertical line beneath and above it, correspondingly. Due to the paper

size limitation, the conductor is too small to see its boundary setting clearly, so that this part is partially enlarged and shown in Figure 3.4.3.

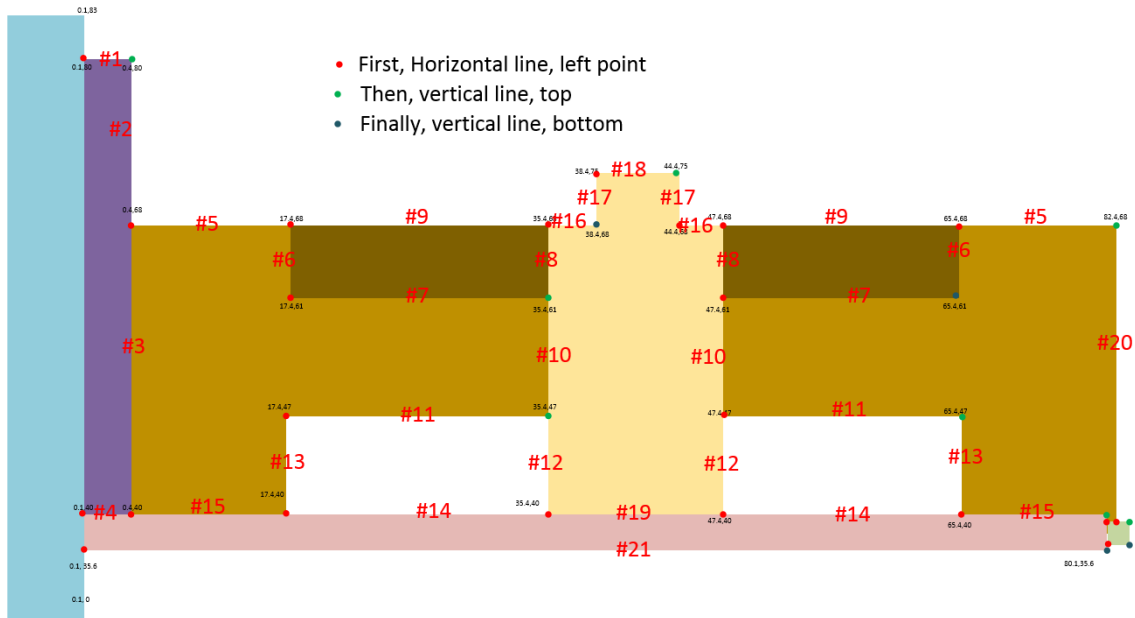


Figure 3.4.2 Boundary Condition Numbering and Category

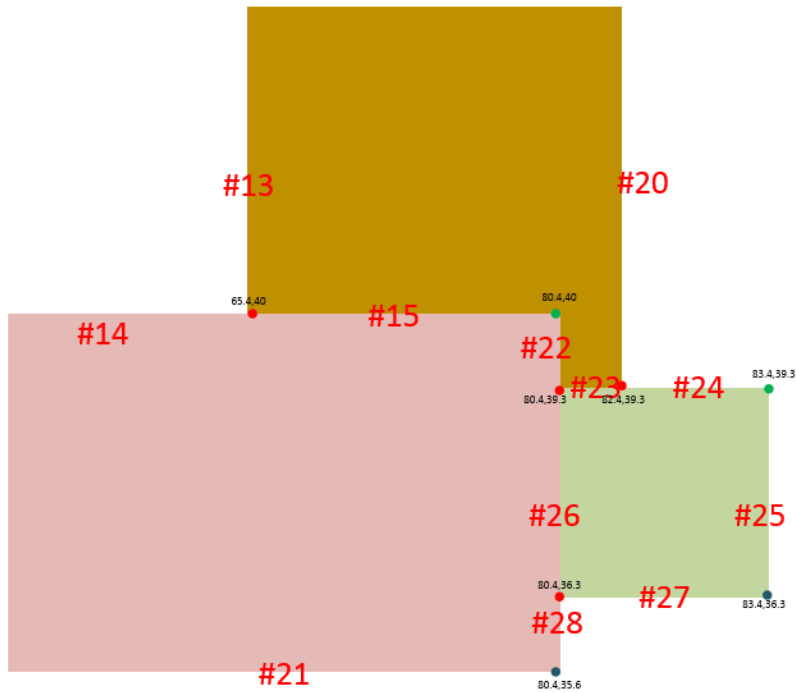


Figure 3.4.3 Boundary Condition Numbering and Category for Conductor

3.5 Case Classification

To rule out the possibility of being electrocuted, three dangerous perching positions of raptors are all supposed to be considered. The first one is that the left wing's tip touches grounded pole and right wing is 3 inches away from the conductor. The second situation assumes left wing 3 inches away from the pole without protection and right wing touching the phase conductor. The final scenario is the left wing touching the raptor guard and right wing touching the conductor. In addition, the dielectric performance when contaminated will be taken into account, too.

In the following section, four cases will be simulated to validate the raptor guard performance under the high voltage threat. The electric field of the Insulator surface and pole surface are exhibited by figures.

3.5.1 Case#1: Left Wing Contact Pole, Right Wing 3 Inches from Conductor

The raptor posture is described in Figure 3.5.1. The primary threat would be the flashover occurring at the right wing's tip which is 3 inches away from the conductor. Figure 3.5.2 and 3.5.3 provide electric field distribution along pole and insulator surface.

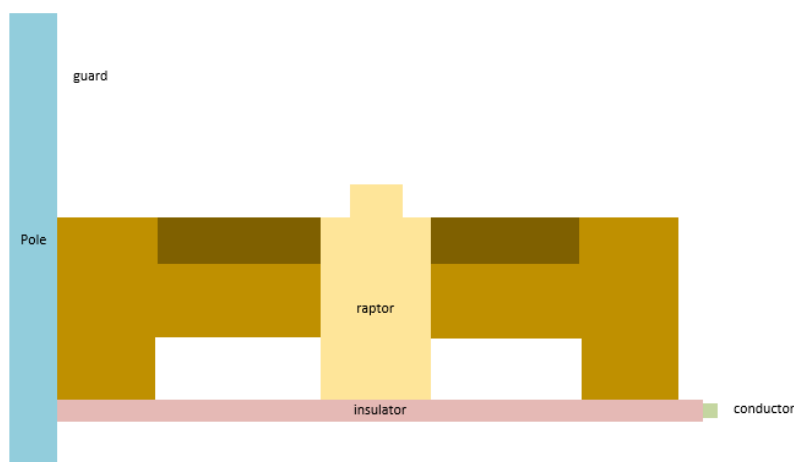


Figure 3.5.1 Case#1 Diagram

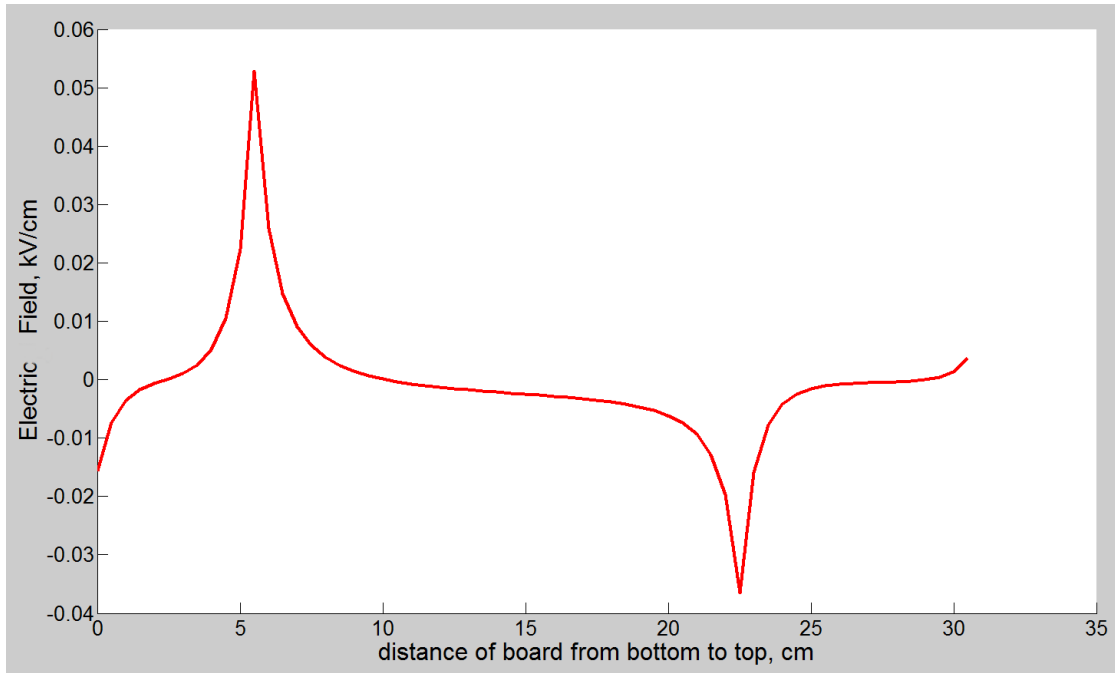


Figure 3.5.2 Pole Surface Vertical EF in Case#1

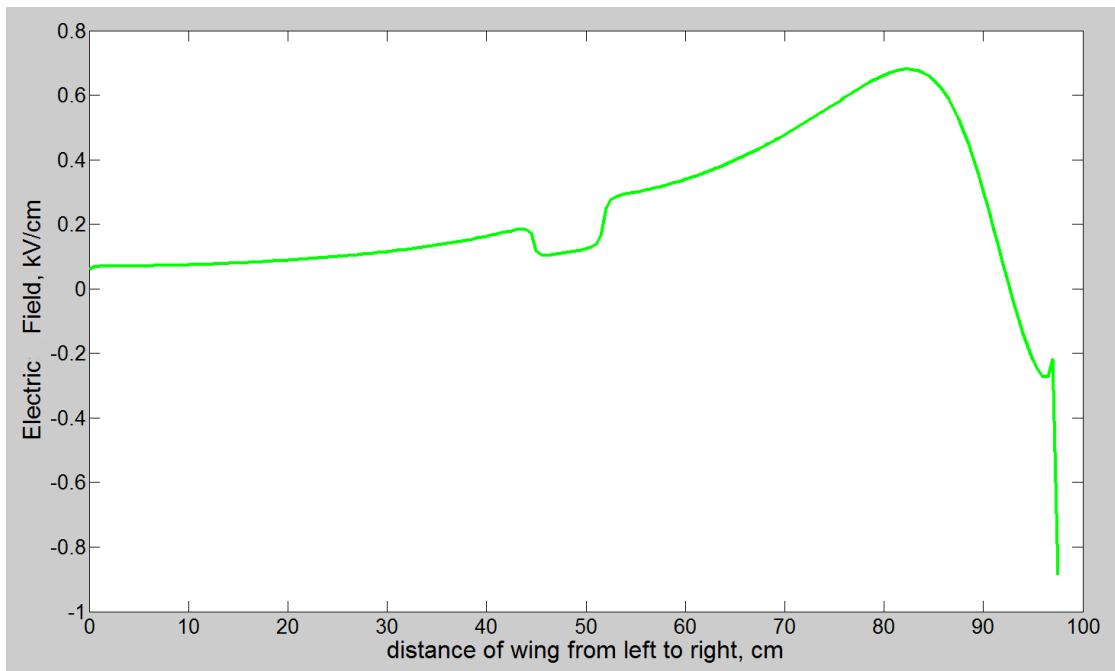


Figure 3.5.3 Insulator Surface Horizontal EF in Case#1

3.5.2 Case#2: Left Wing 3 Inches from Pole, Right Wing Contact Conductor

Similarly, same procedures are repeated except the raptor moves 3 inches right horizontally. In this case, its left wing is 3 inches away from the pole but the right wing

contacts the conductor. Figure 3.5.5 and 3.5.6 describe the electric field at the same position as figures in the previous case.

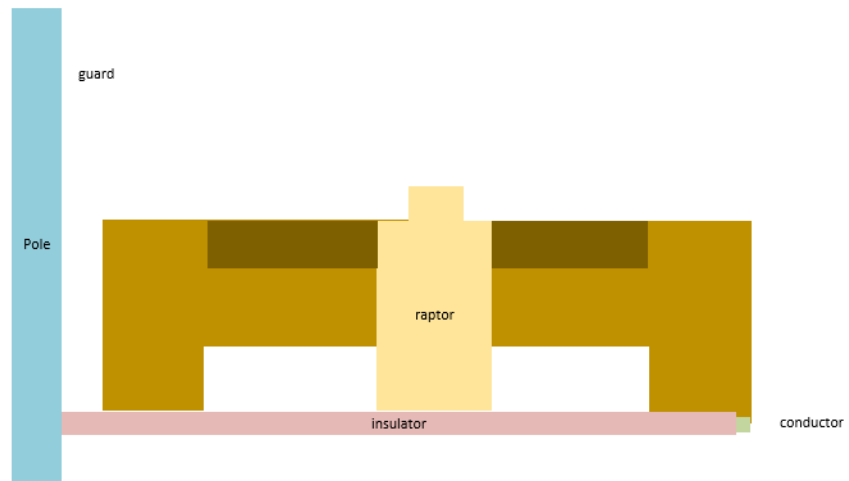


Figure 3.5.4 Case#2 Diagram

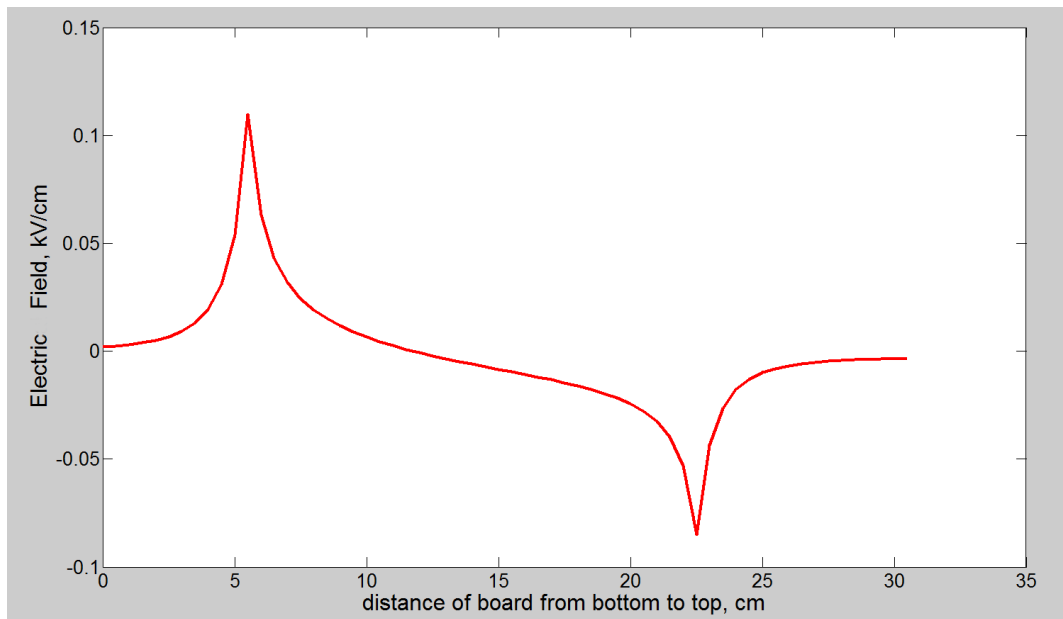


Figure 3.5.5 Pole Surface Vertical EF in Case#2

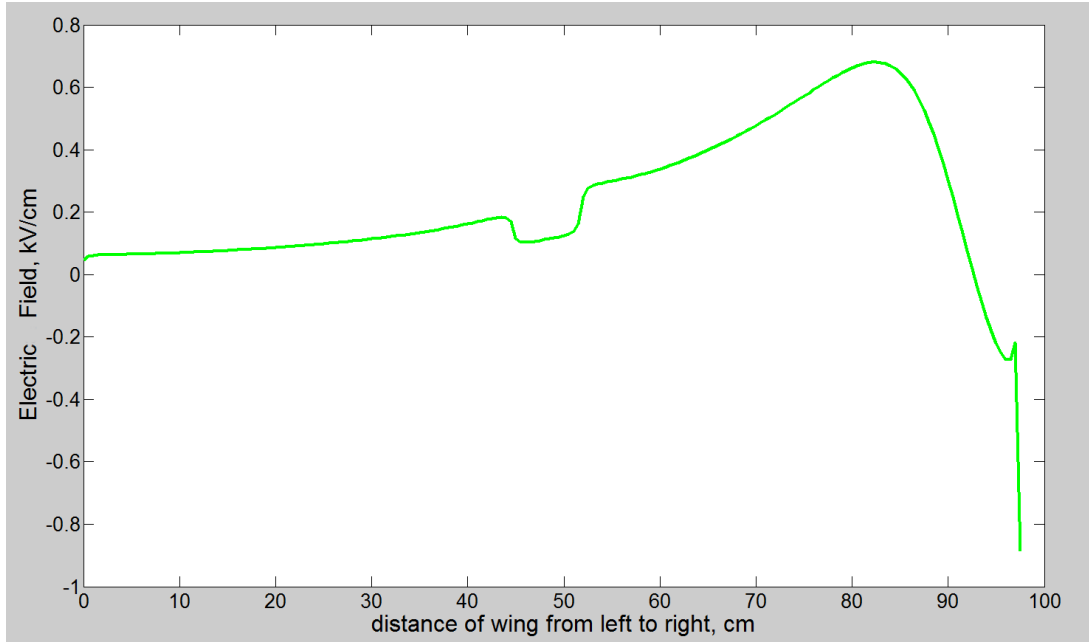


Figure 3.5.6 Insulator Surface Horizontal EF in Case#2

3.5.3 Case#3: Left Wing Contact Guard, Right Wing Contact Conductor

This case mainly focuses on the situation where raptor is exposed to the high voltage. Its left wing touches the raptor guard which is installed on the pole and the right wing contacts the energized conductor. Figure 3.5.8 and 3.5.9 reflect the electric field at this position.

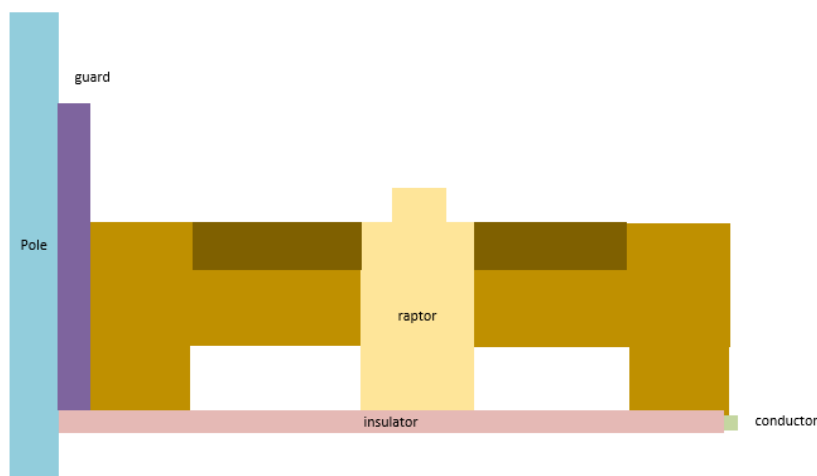


Figure 3.5.7 Case#3 Diagram

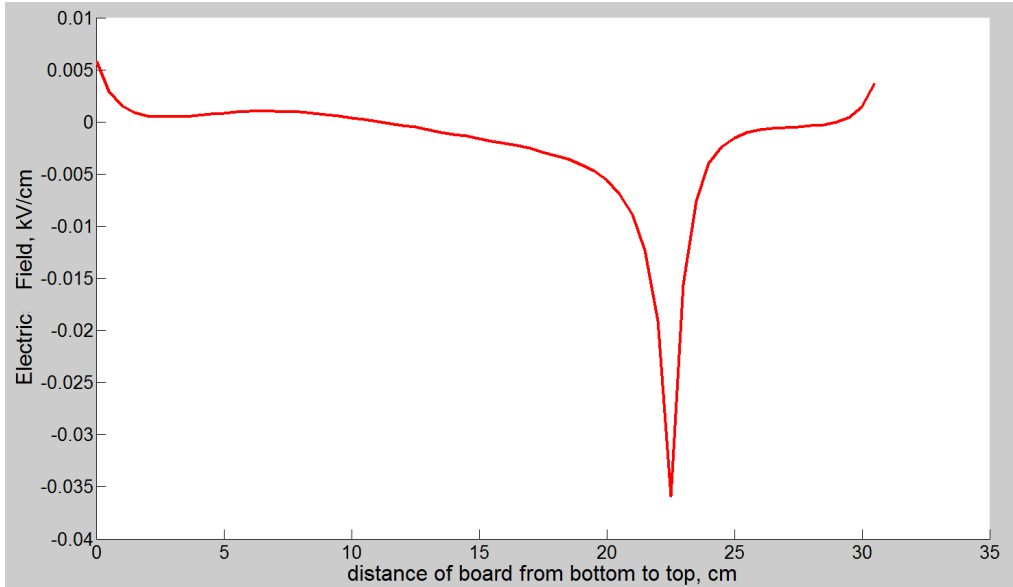


Figure 3.5.8 Pole Surface Vertical EF in Case#3

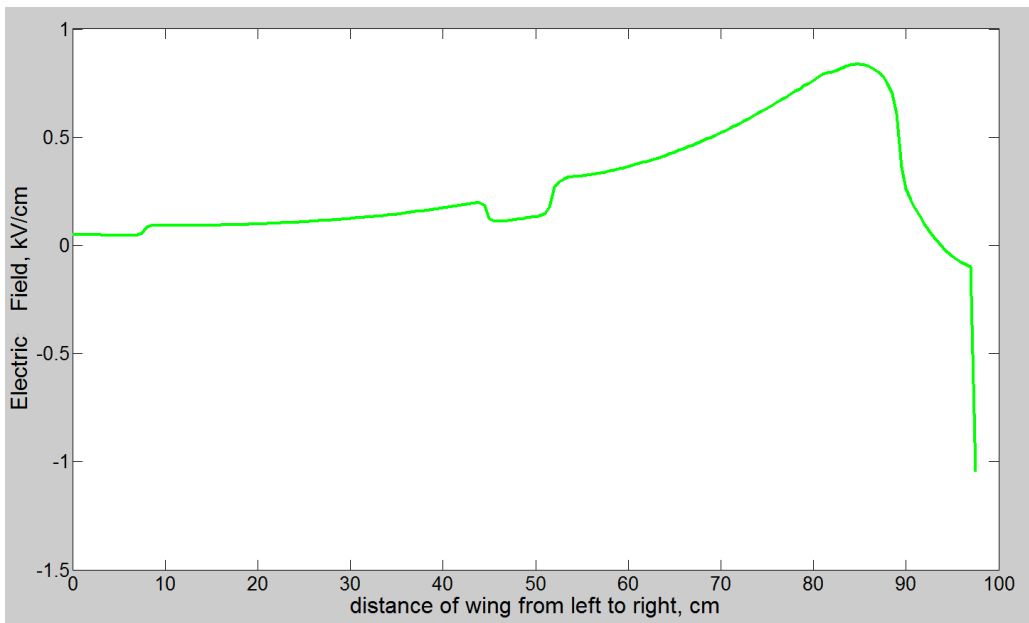


Figure 3.5.9 Insulator Surface Horizontal EF in Case#3

3.5.4 Wet and Dry Comparison

Rain or snow are the common meteorological phenomena in some areas, so it is reasonable to assume these hazardous conditions would happen. Figure 3.5.10 plots the wet condition where all objectives, incorporating the guard, the raptor and the insulator are all covered by water, labeled with the orange color. Figure 3.5.11, 3.5.12, 3.5.13, and 3.5.14

are the electric field along the pole and the insulator surface under the dry and wet condition, respectively.

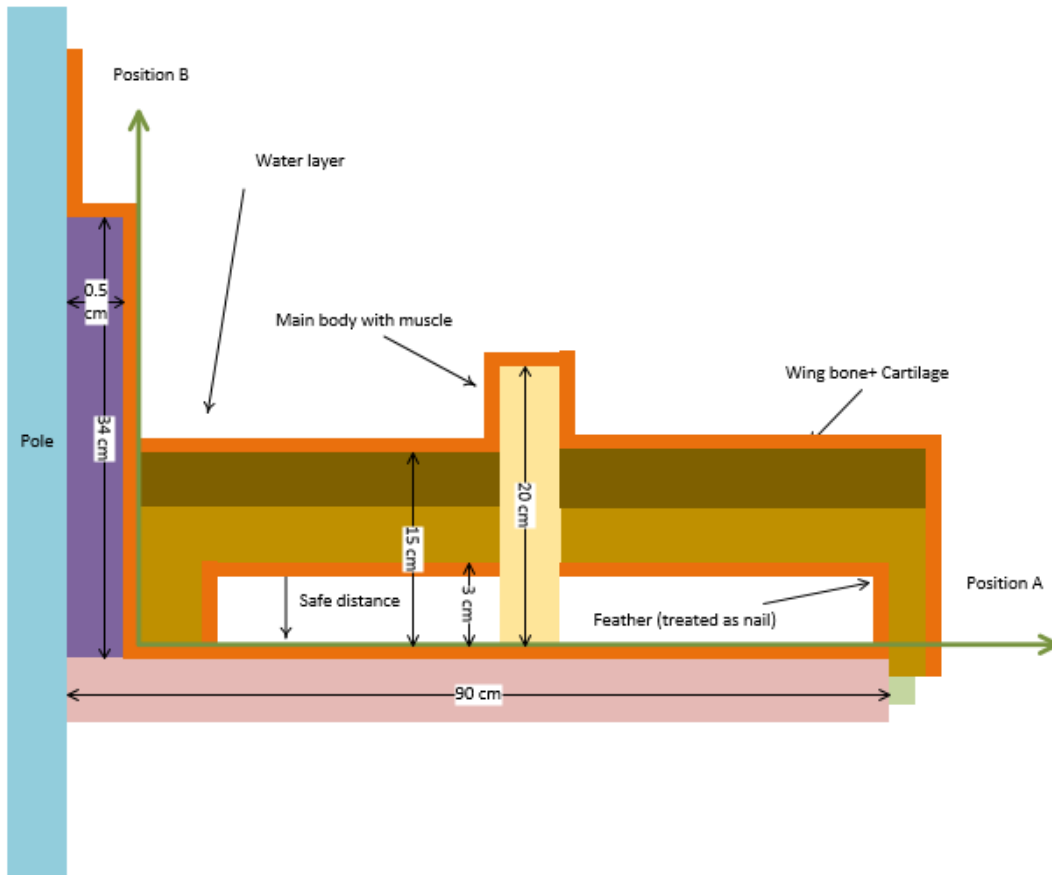


Figure 3.5.10 Wet Condition Diagram

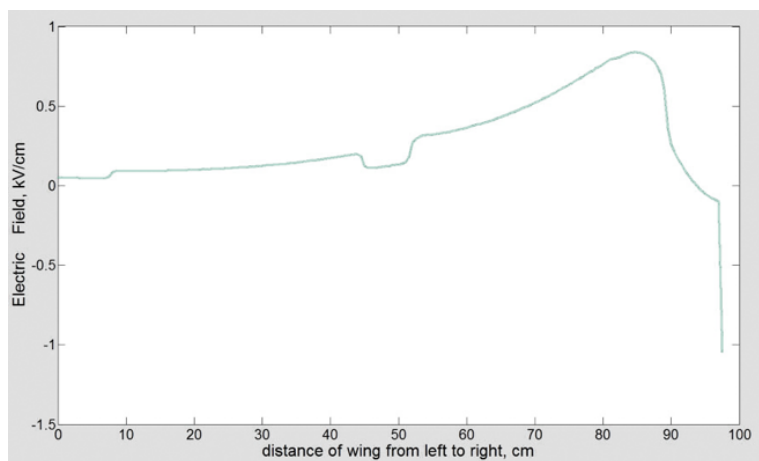


Figure 3.5.11 Insulator Surface Horizontal Electric Field in Dry Condition

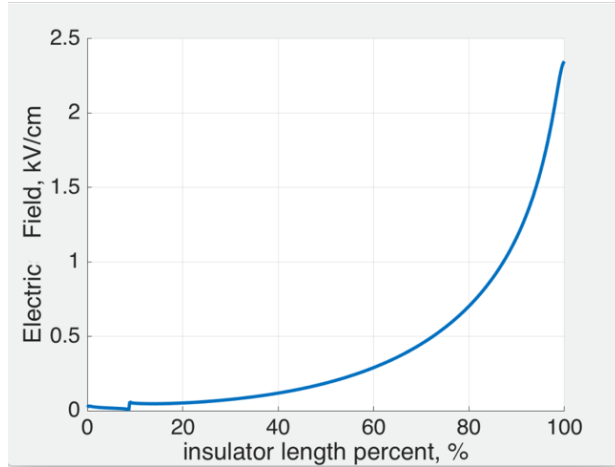


Figure 3.5.12 Insulator Surface Horizontal Electric Field in Wet Condition

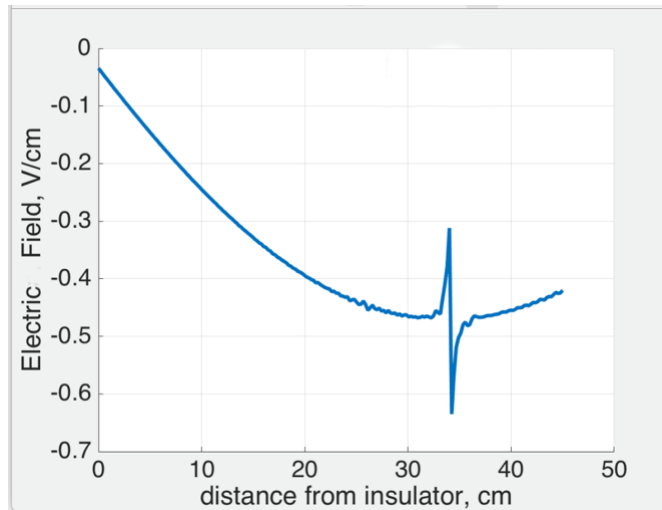


Figure 3.5.13 Pole Surface Vertical Electric Field in Dry Condition

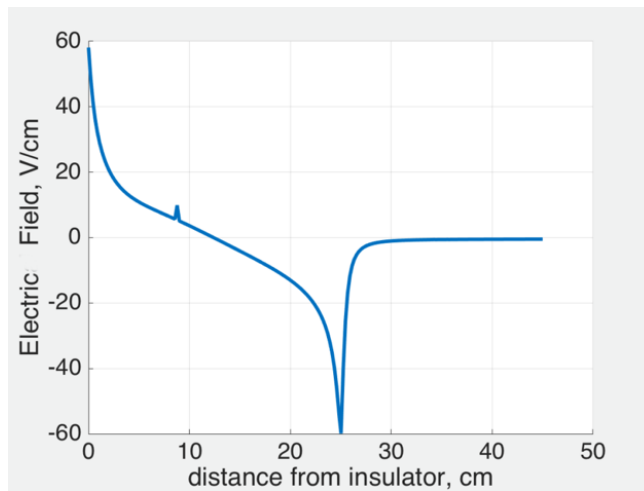


Figure 3.5.14 Pole Surface Vertical Electric Field in Wet Condition

3.6 Result Summary

From the simulation above we may conclude that it is almost impossible to flashover or arc between the conductor and pole when a raptor perches on the insulator, because the limit to puncture air is roughly 20 kV/cm [9] and the electric field in each case are too weak to break down the air in each case. Table 4.3 summarizes the highest potential and electric field at two positions for comparison.

As for the leakage current threat, it will be discussed in Chapter #4.

Table 3.4 Simulation Summary.

Case	Raptor right wing bottom surface		Guard surface	
	Highest Potential (kV)	Highest EF(kV/cm)	Highest Potential (kV)	Highest EF(kV/cm)
#1 Cond away	24.1975	0.6804	0.0943	0.0528
#2 Pole away	24.1988	0.6800	0.3275 Pole surface	0.1097 Pole surface
#3 Guard+cond	38.8101	0.5083	0.0848	0.0368
Wet condition	39.3174	2.3632	0.1062	0.0587

4 EXPERIMENT ON RAPTOR GUARD MATERIAL

4.1 Initial Tracking Voltage Test (ATSM D2303-13)

Several experiments were conducted to test the dielectric characteristics of the raptor guard designed by SRP. The main constituent material is non-waxy polyethylene. This product is selected as an example to provide data for comparison with the simulation result.

ASTM D2303-13 Standard--Liquid contaminant, inclined-plane tracking, and erosion of insulating materials--is adopted to quantitatively evaluate the effects upon an insulating material resulting from the action of electrical discharges [21]. The effects are similar to those that may occur under the influence of dirt combined with moisture condensed from the atmosphere.

To find the initial voltage for the 8-hour tracking test, the initial tracking voltage test is introduced first.

4.1.1 Circuit Diagram

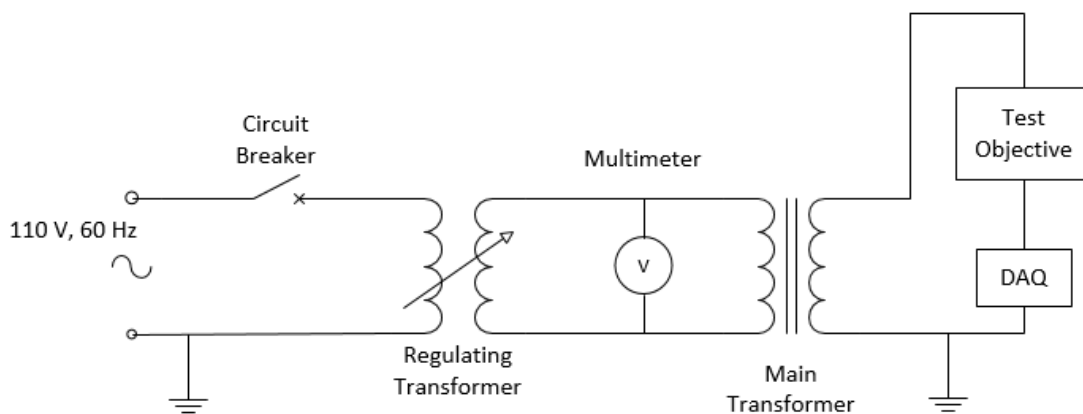


Figure 4.1.1 ITV Circuit Diagram

The power source for this experiment is taken from a 110V AC wall outlet. A regulating transformer rated 15.7 kVA pumps the voltage with the ratio 1:120 to control the input voltage of the main transformer. The multi-meter attached between two phases indicates the low side voltage of the main transformer, which could be converted to the voltage on the sample. To protect devices in the whole circuit, a circuit breaker between two transformers is indispensable. After those, the main transformer with a 240:19920 ratio increases the voltage to a voltage level over a thousand volts. A data acquisition is connected in series with the sample to record the leakage current during the test.

4.1.2 Test Specimens

The raptor guard shield is cut to 120mm×50mm pieces according to the ASTM D2303-13 standard. Each piece has two sides: slick and coarse. Both sides will be tested under the same conditions.

Three holes are necessary to secure the sample on the holder. Position and detailed information are shown in Figure 4.1.2.

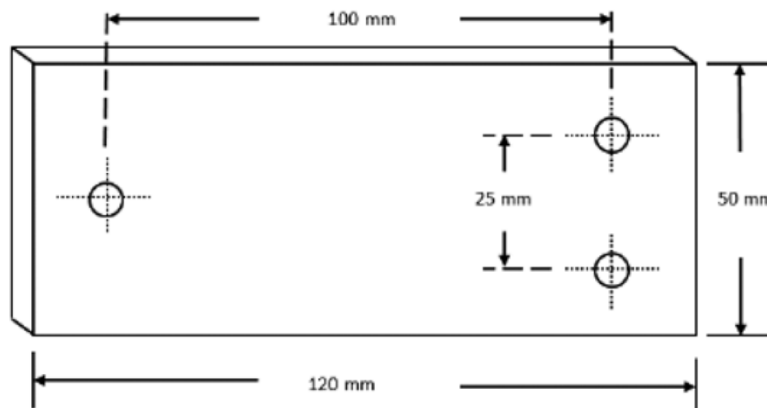


Figure 4.1.2 Raptor Sample Dimension

4.1.3 Specimens' Holder and Irrigation System

To imitate the contaminated situation, an irrigation system which delivers the conductive solution is indispensable. The solution is composed of 0.1% NH₄CL in pure water plus 0.02% wetting (30% Triton). A pump controls the flow rate based on the test voltage. This relationship is indicated in Table 5.1

Table 4.1 Flow Rate Setting

Flow rate of 0.1% NH ₄ CL ml/min	Voltage range, kV	Series resistor Ω
0.075	1 to 1.75	1 000
0.15	2 to 2.75	10 000
0.3	3 to 3.75	50 000
0.6	4 to 4.75	50 000

Two metal electrodes are used to attach the sample on the experimental rack. They provide a conductive contact for the sample. The top electrode is bent at a certain degree for the filter and pipe to be easily installed. Two screws are tightened into corresponding holes on each side. A small semicircle cutout at the bottom may induce the contaminated solution to flow roughly in the same pathway

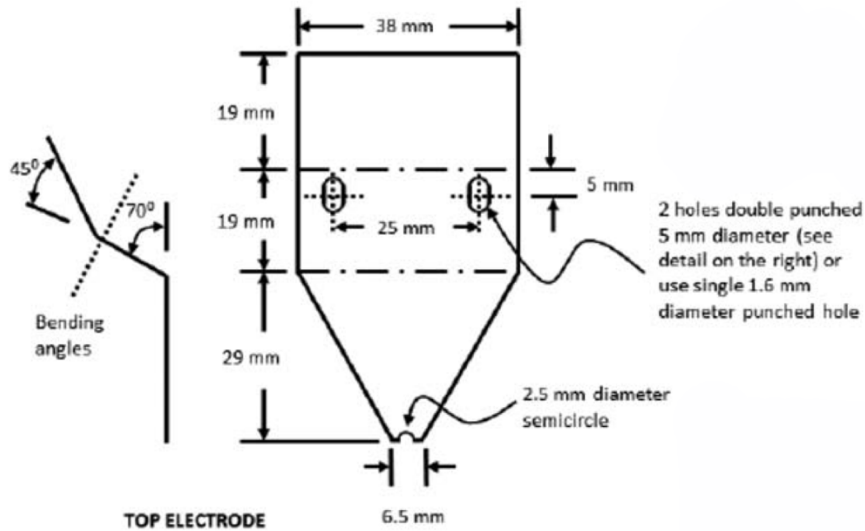


Figure 4.1.3 Top Electrode Diagram

Figure 4.1.4 elaborates the bottom electrode design. Of note is that the bottom electrode is bent toward the sample in an upright position instead of fitting flush to the sample surface.

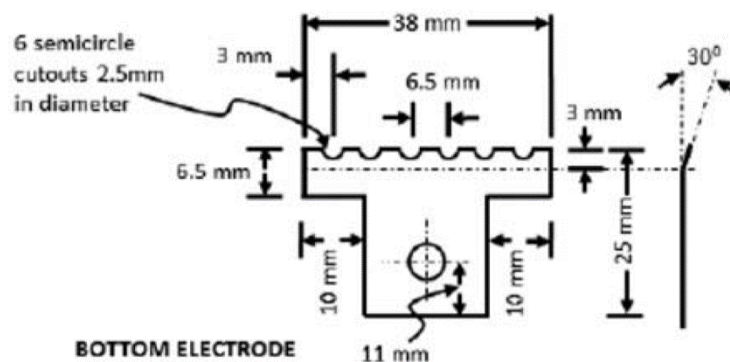


Figure 4.1.4 Bottom Electrode Diagram

A circular filter is folded three times to form an 8-layer tip. Two triangle pieces should be cut out of the middle part of the filter in order to fit into the top electrode. This allows the solution to funnel through the semicircle cutout tip of the top electrode (Figure 4.1.5). A solution delivering hose is placed in the center of the 8-layer filter (Figure 4.1.6). It may take 20 seconds to 1 minute to wet the filter before the solution drips along the sample. Figure 4.1.7 exhibits how to assemble two electrodes and sample.

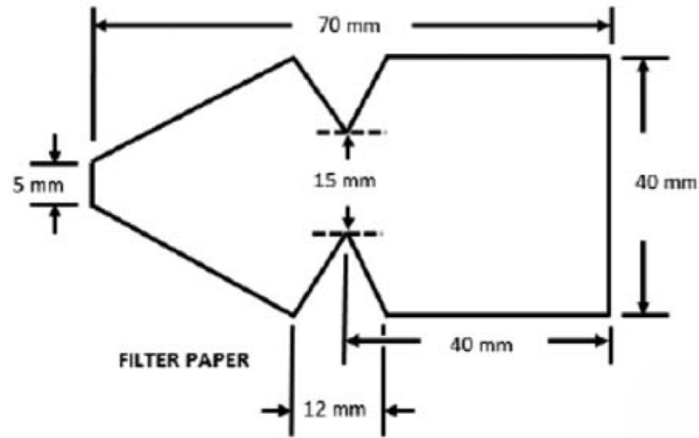


Figure 4.1.5 Filter Paper Dimension

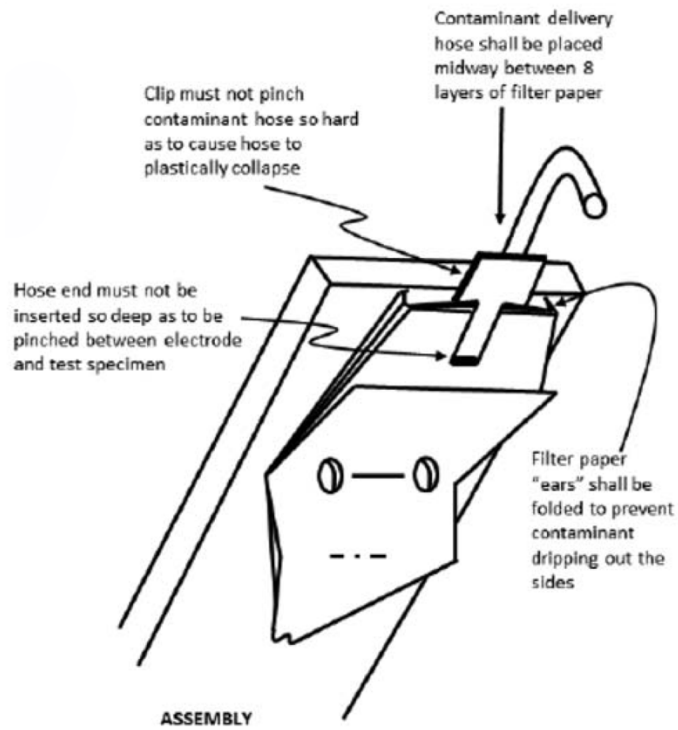


Figure 4.1.6 Top Electrode Assembly

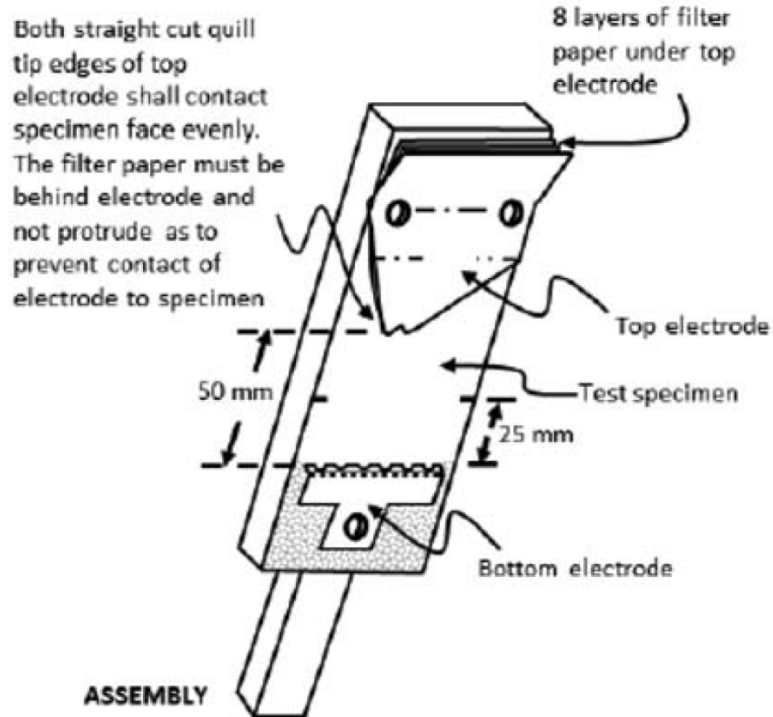


Figure 4.1.7 Holder and Irrigation System Assembly

4.1.4 Procedure

- Prepare contaminant solution (conductivity $2.5 \mu\text{S/cm}$)
- Measure the solution conductivity.
- Fix sample on the truss with electrodes
- Circuit check
- Move out ground rod
- Switch on power and increase voltage to aim value within 15 seconds.
- Increase voltage by 250 V step per hour.
- Record the voltage and the time of tracking.
- Decrease voltage to zero, switch off the power
- Put the ground rod on high voltage end of the transformer.

- Take the sample out.
- Wipe off the sample and take pictures.

4.1.5 Experimental Observation

The experiment started with a slick-side sample under 2.5 kV. There were some slight arcs shown on the surface of the sample at the beginning. Then, about 10-second persistent arc scorched the sample several times (Figure 4.1.8). After roughly 40 minutes, the arc burned so drastically that the sample caught fire entirely (Figure 4.1.9). Some black fluffy fibers remained on the surface of the sample. See Figure 4.1.10.

The second test used a slick-side sample under 2.0 kV. The same phenomenon occurred and the experiment had to be ended after 29 minutes.

The third sample was applied to 2.0 kV on the coarse side. Nothing changed except that the flame occurred at 38 minutes.

To prevent fire, the fourth test only used 1.0 kV on the coarse side. The sample tolerated 1.0 kV and 1.25 kV for 60 minutes respectively. Only some small arcs appeared. When the voltage reached 1.5 kV for 15 minutes, a continuous flickering point moved up from the bottom electrode for roughly 15 seconds, but it was just a point rather than a line. Similar flickering points (not glaring) turned up incessantly, charring the sample's surface. After 2 hours and 44 minutes, the sample caught on fire.

The final test starts from 0.5 kV and nothing occurred within 0.5 to 0.75 kV. When the voltage was raised to 1.0 kV, there were small sparks at the end of an hour period. Obvious tracking occurred under 1.25 kV and finished the full objective distance after 2 minutes under 1.50 kV.

Figure 4.1.11 shows the three samples after the experiment for comparison.

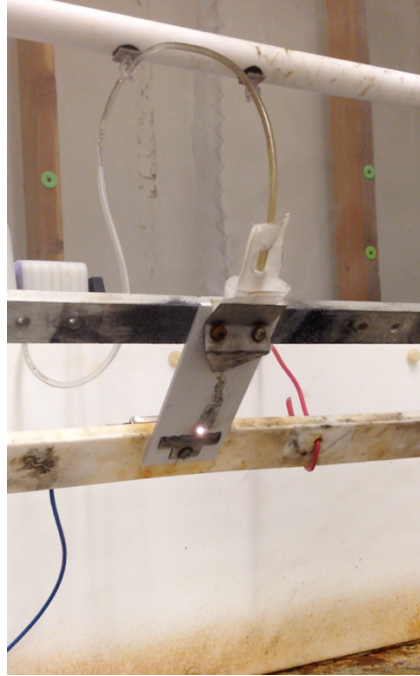


Figure 4.1.8 Tracking during Experiment

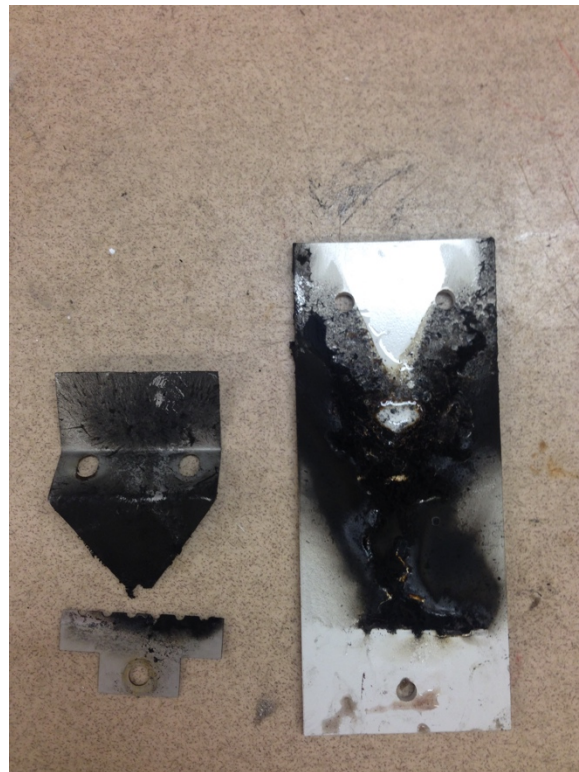


Figure 4.1.9 Raptor Guard Sample after Burning



Figure 4.1.10 Black Fluffy Fibers on Surface



Figure 4.1.11 Tested Sample under Different Period and Voltage

4.1.6 Significance and Use

All the results are summarized in Table 4.2. It is easy to conclude that 1.25 kV or higher voltage may not be an ideal voltage level for the time-to-track experiment, because no sample could survive under this voltage level over 2 hours, but the time-to-track requires an 8-hour unremitting test. The starting voltage for the time-to-track should be the voltage which can endure a 2- or 3-hour test in the initial-tracking-voltage experiment. Sample #6

and #7, which start at 0.5 kV and 1 kV, tolerate the contaminated situation longer than 2 hours. Therefore, 1.0 kV is selected in the following section.

Table 4.2 ITV Result

High Voltage (kV) Surface		Initial Tracking Voltage Test, unit(minute+second)						
		0.5	0.75	1.0	1.25	1.50	2.0	2.5
sample#1	slick							39'32" arc burning, fire
sample#2	slick						29'20" arc burning, fire	
sample#5	coarse						38'41" arc burning, fire	
sample#6	coarse			60', nothing	60', nothing	44' fire		
sample#7	coarse	60', nothing	60' nothing	60'at the end small spark	60' tracking	2', tracking		

4.2 Time to Track Experiment (ATSM D2303-13)

Time-to-track experiment is a persistent test which evaluates the dielectric strength under contaminated condition. The standard time length of this test is 8 hours. If no serious tracking occurs during the period, it proves that the material is qualified to insulate this voltage level.

Devices and procedures applied in this experiment are similar to the previous initial-voltage-tracking experiment. The only difference is that the voltage will be held at a constant value until either the the maximum time length (8 hours) or anytime when a serious tracking or burning happens.

Table 4.3 TTT Result

Time To Tracking				
Surface		Voltage(kV)	Time	Result
sample#1	coarse	1.0	6h10'	tracking
sample#2	slick	0.75	8h nothing	nothing
sample#3	coarse	1.25	4h26'	tracking
sample#4	coarse	0.75	8h	nothing
sample#5	slick	0.75	8h	nothing
sample#6	slick	1.0	8h	nothing
sample#7	coarse	1.25	7h35'	tracking
sample#8	slick	1.75+2.5	3h+1h	nothing

Table 4.3 presents the detailed experimental result. One could conclude that surface type does not exhibit obvious influence on tracking time. In addition, this raptor guard performs a reliable insulative nature under 1 kV, even though in sample #1 a tracking happens after 6 hours, because the discreteness in high voltage experiment should be taken into account. When voltage increases to 1.25 to 1.75 kV, 4 hours looks like a bottleneck for this guard.

However, for the actual situation where a raptor is perching on a horizontal insulator, one could completely assume that no raptor will keep wings spreading over 5 minutes, which is much shorter than the experiment period. It follows that the guard material is supposed to prevent tracking even under 2.5 kV in actual raptor-protection situation.

Moreover, a current monitor is installed at the end of test objective to record the leakage current during the experiment. USB-6008 from the National Instruments is a data acquisition (DAQ) which is compatible with LabView [22]. Detailed specification is listed below:

- Eight analog inputs (12-bit, 10 kS/s)

- Two static analog outputs (12-bit); 12 digital I/O; 32-bit counter
- Bus-powered for high mobility; built-in signal connectivity
- -10 V - 10 V analog input maximum voltage range with 7.73 mV accuracy
- 512 B on-board memory



Figure 4.2.1 NI USB-6008

The sample rate for this DAQ is 5000 points per second, and the sensor resistance is 22.2 ohms. Since the sensor could only collect voltage signal, the leakage current information is originated from the equation where voltage signals are divided by series resistance. All these data are analyzed through MATLAB. The code is attached in the appendix.

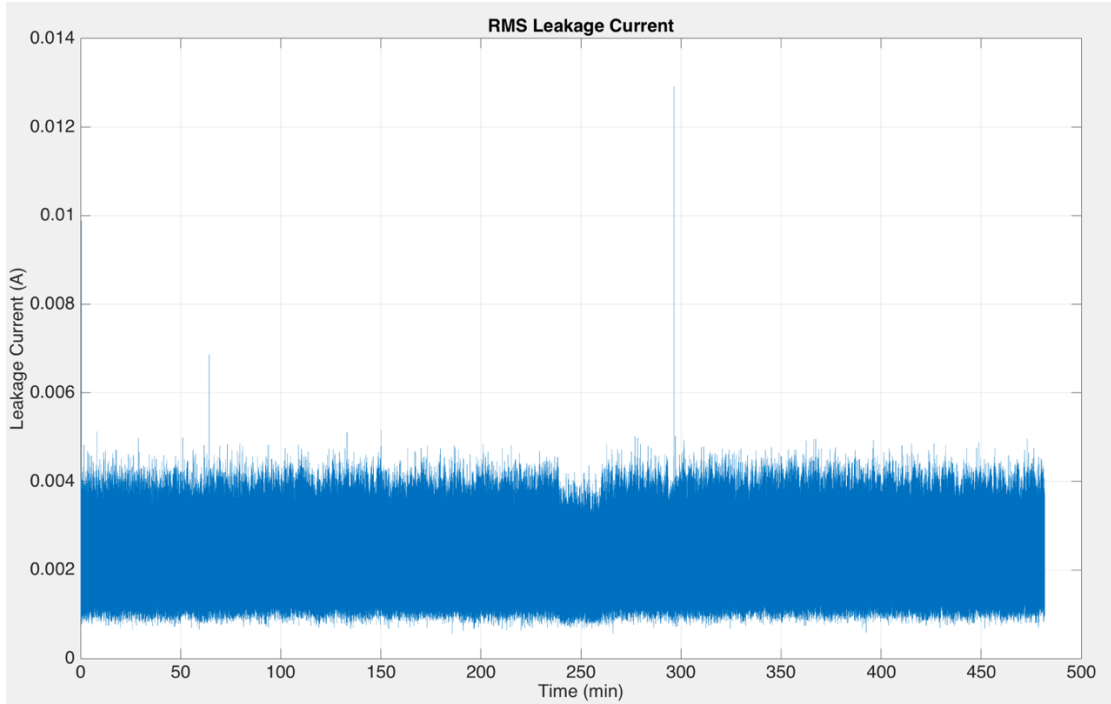


Figure 4.2.2 RMS Leakage Current Data under 750 V

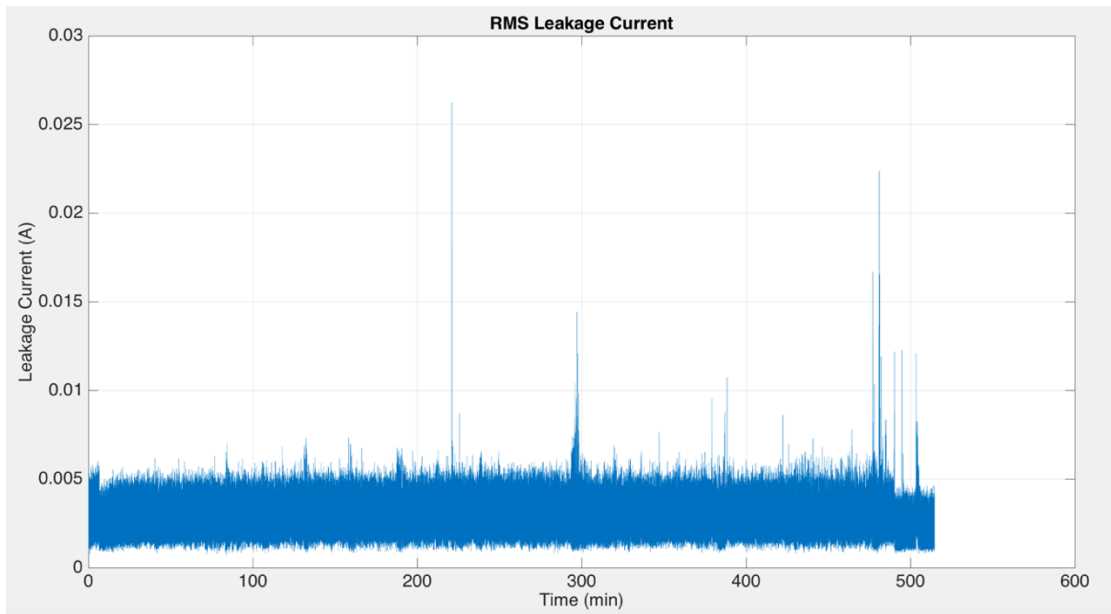


Figure 4.2.3 RMS Leakage Current Data under 1250 V

The two figures above are the root mean square leakage current data of 750 V and 1250 V time-to-track experiments. The horizontal axis represents test time, approximately 480

minutes (8 hours), whereas the vertical axis is the leakage current value with the unit ampere.

When 750V was applied on the sample, the leakage current looks pretty flat and does not change over the long period. The average peak value is roughly equal to 0.004A, almost no arc or tracking occurred during the test.

Once the voltage is increased to 1250V, several spikes exist randomly with a maximum value over 0.01A. During the experiment, some small arcing occurred for less than one second, which may be in accordance with these current data's spikes. In the following test under higher voltage level, more leakage-current spikes are observed. But the average leakage current value, excluding spikes, almost ranges from 0.004A to 0.005A.

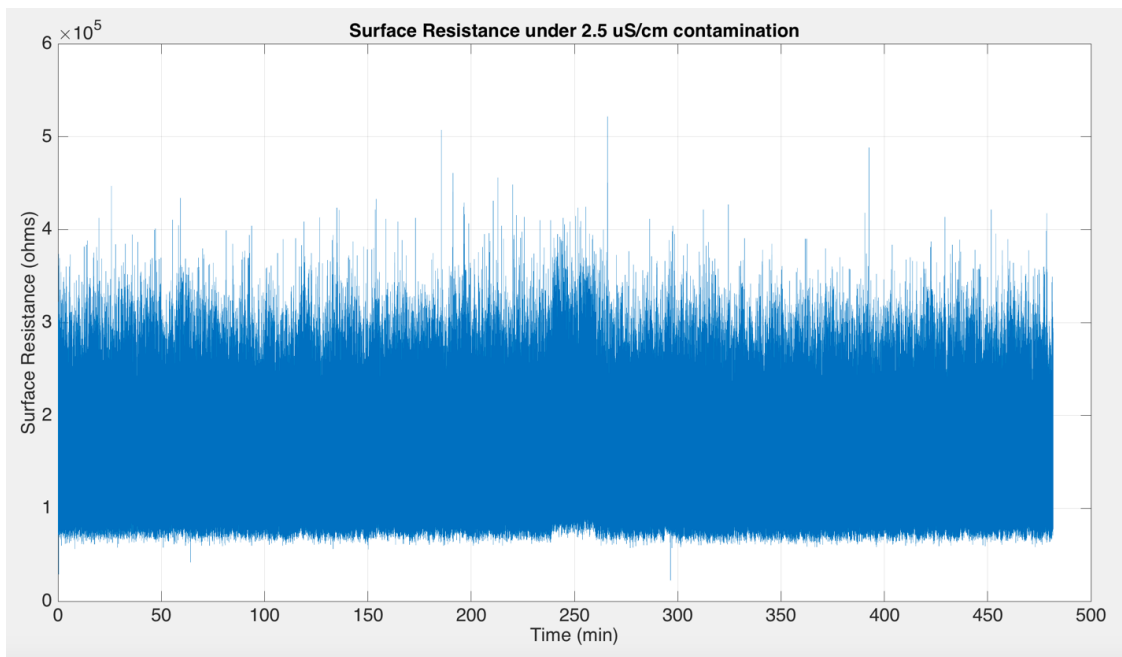


Figure 4.2.4 Surface Resistance Current Data under 750 V

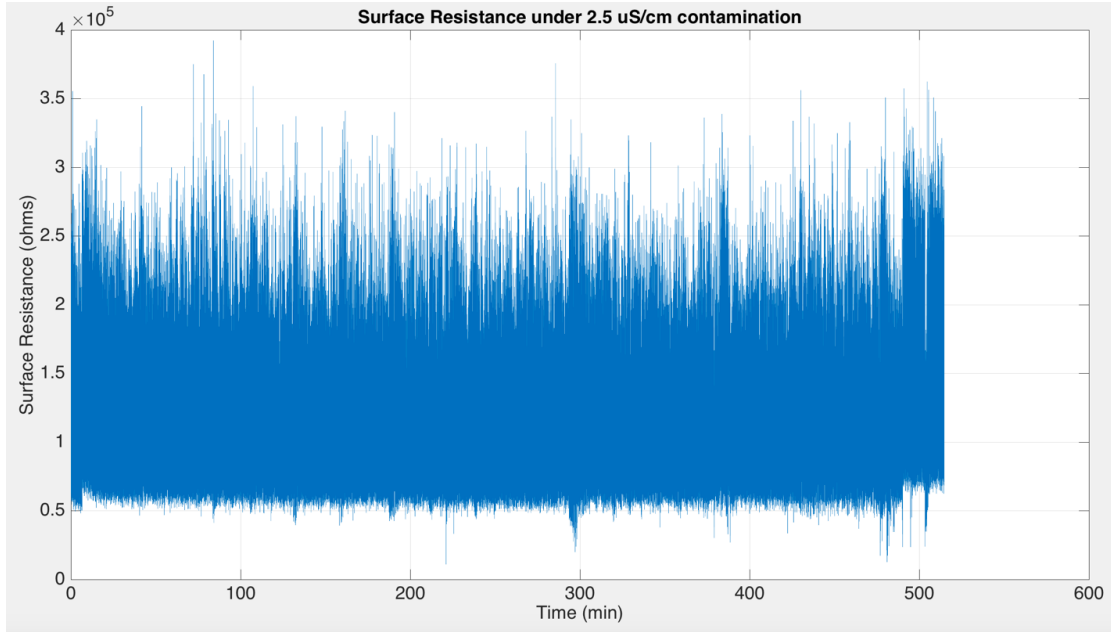


Figure 4.2.5 Surface Resistance Data under 1250 V

Figure 4.2.4 and 4.2.5 provide a real-time example of the surface resistance under 750V and 1250V. The former result behaves steadier over time, which means the resistance remain the same, while the latter one fluctuates more drastically, indicating the sample appears to be changeable according to the external voltage.

If we summarize the result from 750V to 2500V in Table 5.4, it turns out that the RMS leakage currents are almost all 0.004A no matter the voltage level, but the surface resistance floats when voltage changes. Besides, if we gain insight into the leakage current over time, the higher the voltage it applies, the more leakage-current spikes exist. More sense pinnacles presence ought to be expected when the voltage rises.

Table 4.4 TTT Leakage Current and Surface Resistance

voltage level	RMS LC average, A	RMS LC peak, A	Surface R average 1e5	Surface R peak 1e5
750	0.004	0.012	7.79	13.49
1000	0.004	0.018	9.00	16.26
1250	0.005	0.025	10.81	17.30
2500 after 3h 1750	0.004	0.011	25.95	38.93

In conclusion, under the voltage range from 750V to 2500V, this raptor guard is eligible to hold leakage current down to 0.004A for the most time. But a higher voltage may lead to a greater possibility exposing to the arc, which is a death threat for the raptor.

4.3 Dielectric Breakdown Voltage Experiment.

Besides the surface resistance, the breakdown voltage should also be discussed. For a thin material with a huge area, the electric puncture might happen prior to a flashover along its surface. In this situation, the surface resistance could not reflect the real dielectric strength of this material. To rule out this possibility, the dielectric breakdown voltage experiment will be done.

Standard ASTM D149-09 provides the detailed procedure for the dielectric strength of solid electrical insulating materials at commercial power frequencies [23]. The alternating voltage at a commercial power frequency is applied to a test specimen. The voltage is increased from zero or a level well below the breakdown voltage until a dielectric failure of the test specimen occurs.

4.3.1 System Diagram

The circuit of this test is closely similar to the former ITV and TTT test. A modification after two transformers is made to replace a contaminating system by a different sample holder and an electrode in an oil container.

4.3.2 Sample Holder and Electrode

To prevent disruptive electric discharges on the material surface, the whole test should be done in an insulated environment. Figure 4.3.1 shows a bowl (made of non-conductive material) to contain oil. At the bottom, there is a hole which let the ground wire pass through. The plastic rings cover the screw on both sides as the Waterproofing methods.



Figure 4.3.1 Container for Dielectric Oil

The ground electrode is a piece of metal plate. Four screws at corners support the electrode standing above the bowl bottom. A cable tie through two holes fixes the sample on bottom electrode in Figure 4.3.2.

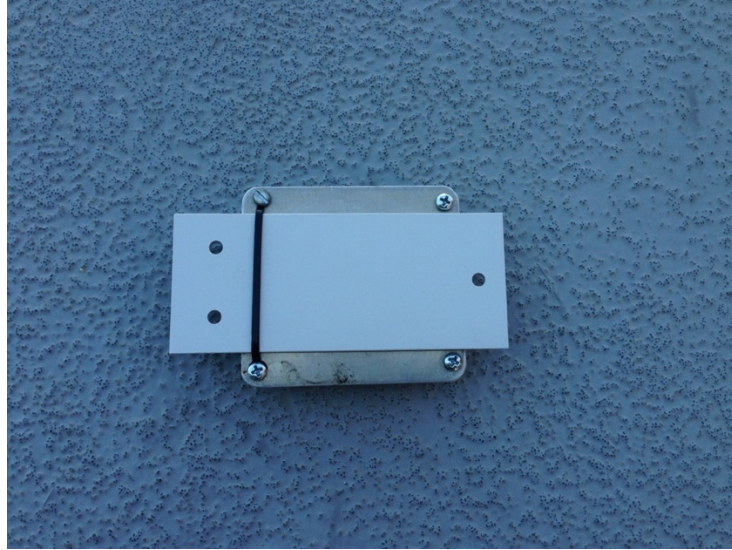


Figure 4.3.2 Sample Attached on Ground Plate

The top electrode is composed of a 15cm long metal cylinder (4mm in diameter) with an edge rounded to 4 mm radius. The wood shelf hangs the electrode over the sample, making them contact tightly. The power source connects the electrode at the other side of the wood in case of an accidental short circuit.

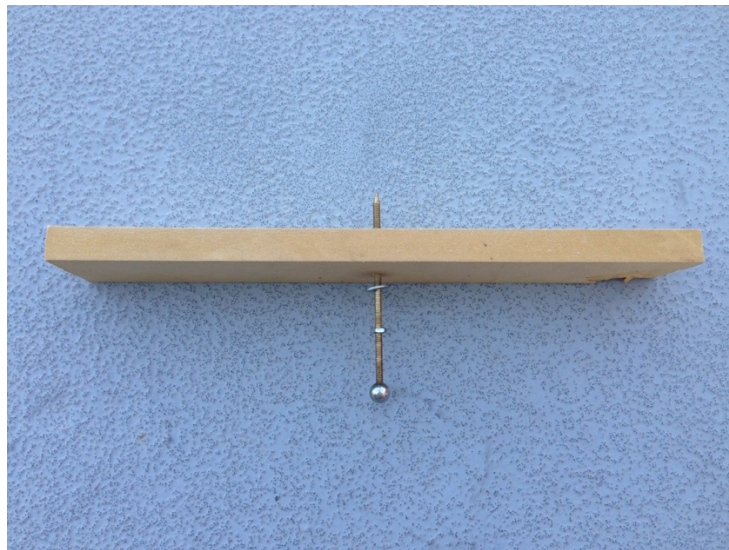


Figure 4.3.3 Energized Top Electrode with A Spherical Contact

Figure 4.3.4 exhibits how these devices work during the experiment. The red clamp is charged at the commercial frequency, while the blue wire is the ground side. Both sample and electrodes are immersed into the dielectric oil.

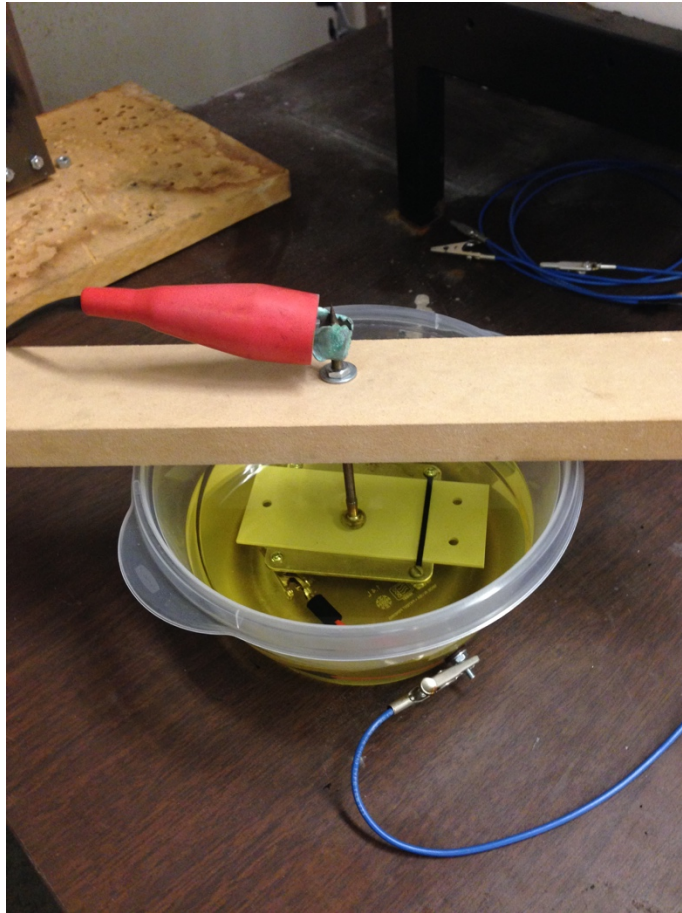


Figure 4.3.4 Sample in the Dielectric Oil

4.3.3 Experiment Procedure

According to the standard, it is desirable that the breakdown occurs in four to ten steps but not less than 120s. Voltage profile of step-by-step test is elaborated in Figure 4.3.5. Each step lasts 60 ± 5 seconds. Initial voltage could be a low level at the beginning, such as 500V. After one or two times, when the breakdown voltage is roughly estimated, then

set an initial voltage four to ten times lower than objective voltage. As for the increment of step voltage, Table 5.5 could be a reference.

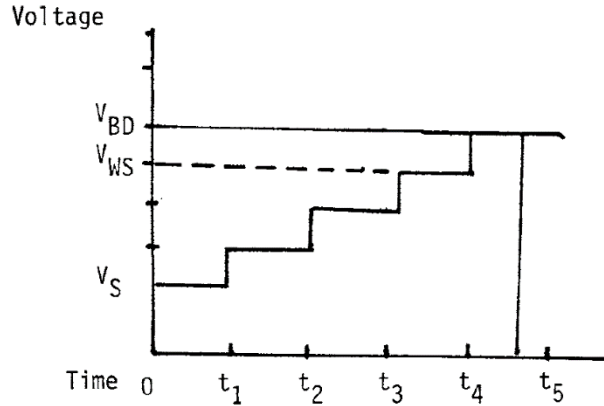


Figure 4.3.5 Voltage Step Profile

Table 4.5 Step Voltage Setting

When initial voltage V_s is (kV)	Increment (kV)
5 or less	10% of V_s
5 to 10	0.5
10 to 25	1
25 to 50	2
50 to 100	5
over 100	10

4.3.4 Experiment Result

Since the time length is much shorter than ITV and TTT, the initial voltage from 2 kV should be reasonable for a 60-second period. Nothing happened after five steps, so the voltage was jumped to 10 kV directly, and still no phenomenon occurred. Finally, the maximum output of the main transformer 15 kV was applied to it for 60 seconds, neither puncture nor flashover existed in the oil. Owing to the upper limit of devices, a higher voltage test could not be finished. The conclusion so far is this material breakdown voltage is greater than 15 kV.

4.4 Voltage Tolerance Test on the Golden Eagle

On February 13th, August 2nd, 1978 and February 6th, 1979, a researcher named Morlan Nelson and his team launched a research to determine the natural capacity of eagles to resist electrocution under various voltage, contact types, and climatic conditions [24] – [26]. A current monitor was attached to a live golden eagle. The purpose is to find how much current flow through the raptor may cause its uncomfortable reaction.

They divided the experiment into two parts. Since feathers on the wing show a better dielectric nature compared with the flesh, two comparison groups have been set. First of all, researchers added a voltage on the wing feathers at various spacing, specific results are recorded in Table 5.6. “n/c” means no measurable current in milliamperes, also no obviously unwell behavior of raptors.

Table 4.6 Result of the Molted Golden Eagle Wing Feathers

Voltage (kV)	Result for electrode spacing (inches)				
	18	14	10	7	5
10	n/c	n/c	n/c	n/c	n/c
30	n/c	n/c	n/c	n/c	n/c
50	n/c	n/c	n/c	n/c	Feather burned at 55 kV
70	n/c	n/c	n/c	n/c	

It turns out that feathers can tolerate high voltage if the spacing between two electrodes is long enough. Only when the voltage rises to 55 kV at a 5-inch gap, the feathers are faced with the danger. In 69 kV sub transmission system, most insulator length is over 35 inches, much longer than the limit length in this experiment, let alone 55 kV is already above 40 kV of the phase-to-ground voltage level. Thus, feather contact for golden eagles should be safe.

The second test was putting electrodes on the flesh, including wing joints and toes. These parts have higher conductivity, faced with more risk from energized devices. Table 5.7 and 5.8 indicate the result in terms of current.

Rather than kilovolt-level tolerance in the feather group, flesh cannot hold voltage over 300 volts. This test had to be terminated at 480 V or even lower voltage, because the raptor has already shown a painful reaction. For the security consideration, the researcher stopped increasing voltage. It proves that the maximum limit for the flesh-contact would be only 400 V level, give or take 30 volts.

Table 4.7 Current of Golden Eagle When Electrodes Attached on Wing Joints

Voltage (V)	Current between wing joints (milliamperes)	
	Test #1	Test #2
60	2	2
120	3	3
160	4	4
200	4.5	4.5
240	5.5	5.5
280	6.5	6.3
320	7.5	7.3
360	8.3	8.1
400	9.3	
440	10.0	
480	11.0	

Table 4.8 Current of Golden Eagle When Electrodes Attached on Toes

Voltage (V)	Current between toes (milliamperes)
60	2
120	3
160	4
200	4.5
240	5.5
280	6.3
320	7.3

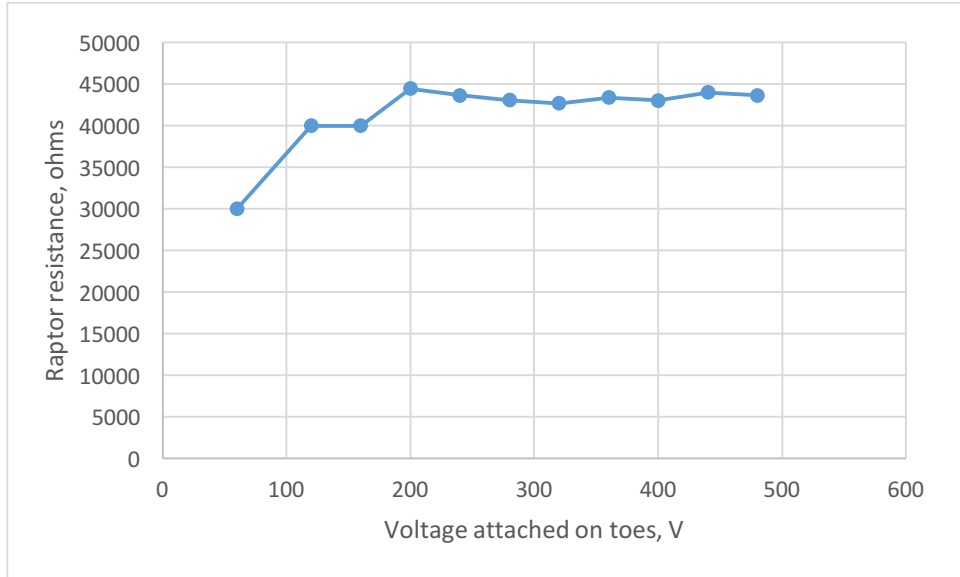


Figure 4.4.1 Raptor Bio-Impedance Estimation between Toes

If the raptor body could be assumed as a pure conductor, its bio-impedance can be calculated by Ohm’s law. Figure 4.4.1 shows the raptor bio-impedance vs. test voltage plot of the previous experiment. It is easy to observe that after voltage goes up to 240 V, the body resistance stabilized at 44, 000Ω. Scientific explanation of this phenomenon cannot be given in this thesis due to the research direction, but we might conclude that for large-size raptors, its bio-impedance magnitude may locate at the ten thousand level.

5 CONCLUSION AND FUTURE WORK

5.1 Conclusion

Computer simulations and dielectric experiments validate the assertion that the raptor guard reduces the potential risk of both debilitating and lethal electrocution of local wildlife to a satisfactory level.

This body of work demonstrates this method decreases the electric field strength at both the pole and the conductor sides, reducing the possibility of flashover. The highest electric field near either the conductor or the guard is below 1kV/cm, which is much lower than 20 kV/cm of theoretical flashover EF. As for the potential, the highest value would only be 400 V near the pole side.

Furthermore, this guard limits the strength of the leakage current below the golden eagle tolerance (8.1 mA in Table 5.1) before they display any sign of discomfort. The maximum leakage current is 5 mA on the material surface if the applied voltage is lower than 2.5 kV. For the potential lower than 400V at the raptor guard, according to the simulation, it is expected the number of raptor bodies near the metal poles should decrease significantly.

Though it is impossible to guarantee the dielectric performance of other utilities' productions are the same due to the material property, the design of the raptor guard is expected to be practically feasible.

5.2 Future Work

5.2.1 Slit Problem between Two Boards

The current SRP raptor guard is composed of several pieces of the polyethylene board with long narrow slits between the board junctions. In the extreme scenario, a raptor's feather may go across the slit, contacting the grounded metal pole directly.

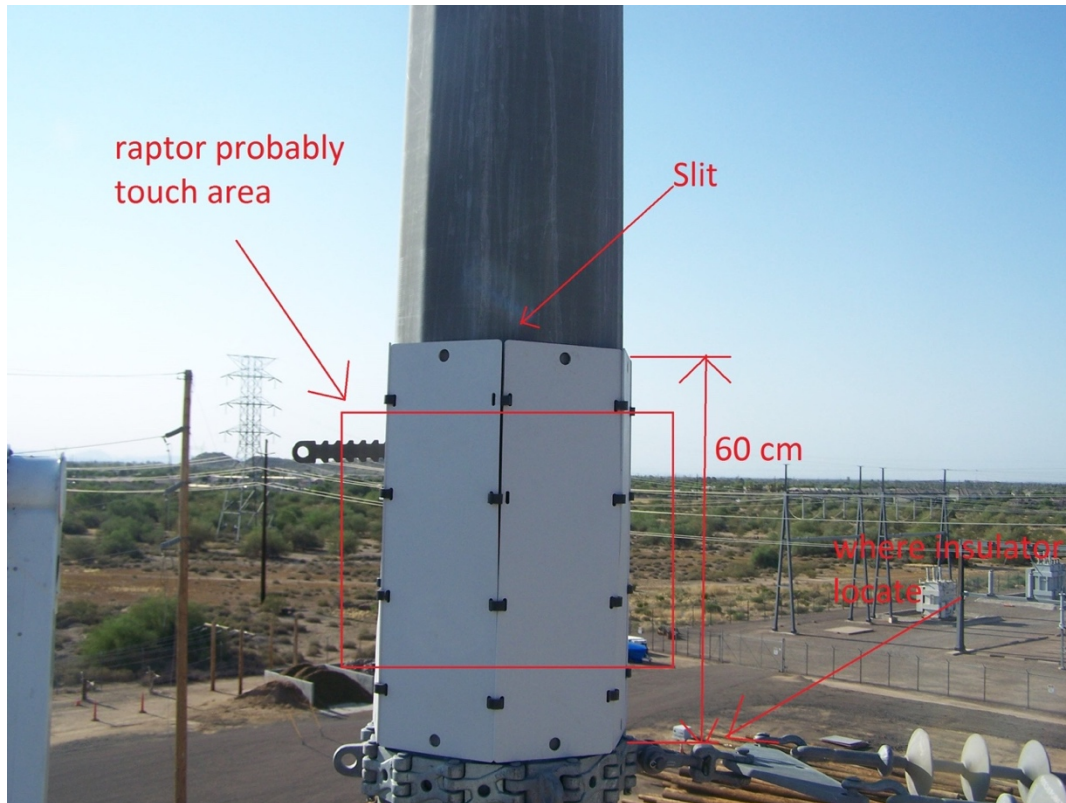


Figure 5.2.1 Slit at the Junction

Furthermore, the slit may affect the dielectric strength in the vicinity of the raptor guard. Usually the dielectric material like polyethylene is difficult to be punctured under 69 kV. A flashover is expected to occur along the material surface rather than go through it directly. The closer the energized part gets to the board's edge, the higher possibility a flashover occurs. Therefore, a flashover experiment to test out the safe distance to the edge might be necessary.

The experiment diagram is shown below. Suppose a situation where we use a metal needle or rod to mimic the wing tip. 40 kV voltage (phase-to-ground voltage in 69 kV system) is charged to the needle tip, while the other side is the guard sample attached on a grounded metal plate, a substitution of the pole. The flashover distance will be explored by moving the needle above the sample in various gaps, such as 0.5 cm, 1 cm, 1.5 cm and so on. Each gap is supposed to be tested over 5 times because the result's discreteness in the high voltage experiment cannot be neglected. If a flashover happens in a specific distance over several times, it proves that under this distance, the electrocution by air puncture is expected, otherwise the raptor should be safe.

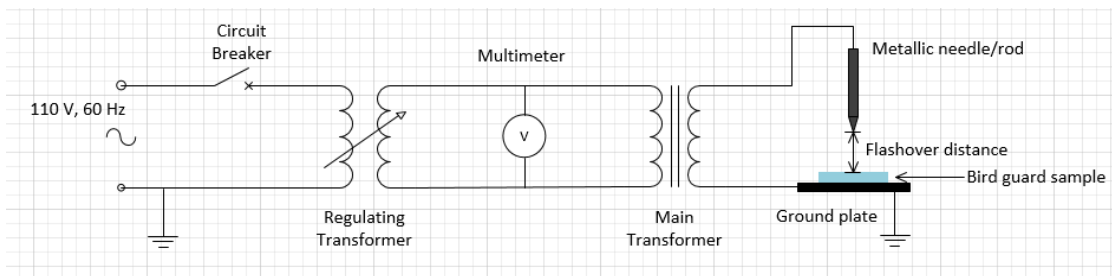


Figure 5.2.2 Flashover Experiment Diagram

Meanwhile, some comparisons need to be done when the metal needle hangs over the central position of the guard and over the guard edge. According to the minimum distance principle, a flashover prefers to occur in a pathway as short as possible. Above the edge, ionized particles do not have to bypass the raptor guard, which results in a higher electrocution possibility. This comparison may gain insight into whether this slit affects dielectric strength.

However, owing to the simulation result (in Chapter #3), the presence of a raptor does not affect a lot on the electric field if it does not contact the pole directly. Using a dielectric tape to cover these slits should be a reasonable option.

5.2.2 Simulation Efficiency

The main disadvantage of finite difference method is about efficiency. Depending on the matrix size, the simulation time length may vary greatly. One example would be the capacitor model whose matrix is only 100×100 , or in other words, 10,000 points in each iteration. It usually takes 5 minutes to get a result within the error tolerance by a computer with an i5 processor and 8 GB memory. However, if the raptor model is applied, a 450×900 matrix will compute 405,000 points per cycle. For the error smaller than 0.05%, it increases the number of iteration two orders of magnitude, which might be 8 hours in terms of time for the same computer. Thus, how to optimize the code is an important objective to improve computing efficiency.

5.2.3 3D Model

Reality is three dimensional instead of a plain world, and the asymmetry of the raptor in other directions (normal to the simulation plain in Chapter #4) also has an influence on the potential and electric field distribution, though it is challenging to say to what extent it will affect the simulation result. In stereoscopic space, the insulator is axial symmetrical, perhaps a 3D model may not increase the accuracy, whereas the raptor, pole and conductor is not as ideal as an insulator, the error originated from these three objectives should not be neglected.

3D is not only difficult to derivate the mathematical model, but also time-consuming in simulation. The total time length will grow exponentially, which is similar to the efficiency problem mentioned in the previous section.

REFERENCE

- [1] Burnham, J., Carlton, R., Cherney, E. A., Couret, G., Eldridge, K. T., Farzaneh, M., ... & Siegel, S. (2004). Preventive measures to reduce bird-related power Outages-part I: Electrocutation and collision. *IEEE Transactions on Power Delivery*, 19(4), 1843-1847.
- [2] Sundararajan, R., Burnham, J., Carlton, R., Cherney, E. A., Couret, G., Eldridge, K. T., ... & Siegel, S. (2004). Preventive measures to reduce bird related power outages-part II: Streamers and contamination. *IEEE transactions on power delivery*, 19(4), 1848-1853.
- [3] Avian Power Line Interaction Committee. Suggested practices for avian protection on power lines: the state of the art in 2006. Edison Electric Institute, APLIC, and the California Energy Commission, Washington, DC and Sacramento, CA (2006).
- [4] Taklaja, P., Hyvonen, P., Kluss, J. V., Niitsoo, J., & Palu, I. (2014). Preventing Bird Streamer Outages Using Alternative Tower Configurations. *IEEE Transactions on Power Delivery*, 5(29), 2402-2409.
- [5] Göcsei, G., Németh, B., Cselkó, R., & Berta, I. (2014, May). Bird protector-related issues on medium voltage overhead networks. In *Live Maintenance (ICOLIM), 2014 11th International Conference on* (pp. 1-6). IEEE.
- [6] IEEE Power and Energy Society, IEEE guide for reducing bird-related outages IEEE Std 1651-2010, New York, NY 10016-5997, 2011
- [7] Guangzheng Ni, Shiyong Yang, Xiuying Qian, Jie Qiu, *Electromagnetic field calculation in engineering*, Machinery Industry Press, Beijing, 2004.
- [8] Takuma, T., Kawamoto, T., & Fujinami, H. (1981). Charge simulation method with complex fictitious charges for calculating capacitive-resistive fields. *IEEE Transactions on Power Apparatus and Systems*, (11), 4665-4672.
- [9] He, J., & Gorur, R. S. (2014). Charge simulation based electric field analysis of composite insulators for HVDC lines. *IEEE Transactions on Dielectrics and Electrical Insulation*, 21(6), 2541-2548.
- [10] Doshi, T., Gorur, R. S., & Hunt, J. (2011). Electric field computation of composite line insulators up to 1200 kV AC. *IEEE Transactions on Dielectrics and Electrical Insulation*, 18(3), 861-867.
- [11] MacLean Power Systems, "Insulator System Catalog", May 2010.
- [12] Italian national research council, Dielectric properties of body tissues in the frequency range 10 Hz to 100 GHz, online resource, available at: <http://niremf.ifac.cnr.it/tissprop/#appl>

- [13] Settle, R. G., Foster, K. R., Epstein, B. R., & Mullen, J. L. (1980). Nutritional assessment: whole body impedance and body fluid compartments.
- [14] Foster, K. R., & Lukaski, H. C. (1996). Whole-body impedance--what does it measure?. *The American journal of clinical nutrition*, 64(3), 388S-396S.
- [15] Phillips, A. J., Childs, D. J., & Schneider, H. M. (1999). Aging of nonceramic insulators due to corona from water drops. *IEEE Transactions on Power Delivery*, 14(3), 1081-1089.
- [16] Que, W., & Sebo, S. A. (2001). Electric field and potential distributions along non-ceramic insulators with water droplets. In *Electrical Insulation Conference and Electrical Manufacturing & Coil Winding Conference, 2001. Proceedings* (pp. 441-444). IEEE.
- [17] Sutherland, P. E., Dorr, D., & Gomatam, K. (2005, May). Human current sensitivities and resistance values in the presence of electrically energized objects. In *IEEE Systems Technical Conference on Industrial and Commercial Power 2005*. (pp. 159-167). IEEE.
- [18] Malek Laissaoui, A., Nekhoul, B., Poljak, D., Kerroum, K., & Drissi, K. E. K. (2014, September). Current density and internal electric field in a model of the human body exposed to ELF electric and magnetic fields. In *2014 International Symposium on Electromagnetic Compatibility* (pp. 974-979). IEEE.
- [19] El Dein, A. Z., Wahab, M. A., Hamada, M. M., & Emmery, T. H. (2010, June). Computation of electric field and human body induced current under overhead transmission lines. In *Systems Signals and Devices (SSD), 2010 7th International Multi-Conference on* (pp. 1-6). IEEE.
- [20] LaForest, J. J. *Transmission-line reference book. 345 kV and above*. No. EPRI-EL-2500. General Electric Co., Pittsfield, MA (USA). Large Transformer Div.; General Electric Co., Schenectady, NY (USA). Electric Utility Systems Engineering Dept., 1981.
- [21] American Section of the International Association for Testing Materials, ASTM D2303-13 *Standard Test Methods for Liquid-Contaminant, Inclined-Plane Tracking and Erosion of Insulating Materials*, West Conshohocken, PA, 2013
- [22] National Instruments, USB-6008 specifications, online resource, available at: <http://sine.ni.com/nips/cds/view/p/lang/en/nid/201986>
- [23] American Section of the International Association for Testing Materials, ASTM D149-09(2013) *Standard Test Method for Dielectric Breakdown Voltage and Dielectric*

Strength of Solid Electrical Insulating Materials at Commercial Power Frequencies, West Conshohocken, PA, 2013

[24] Morlan W. Nelson & Associates, power lines progress report on eagle protection research, 1979b, unpublished, rep Boise, ID. 13pp

[25] Morlan W. Nelson, update on eagle protection practices, 1980c, unpublished, raptor management information system.

[26] Morlan W. Nelson, Power lines and birds of prey, 1976, unpublished, Idaho wildlife revised.

APPENDIX A
CODE FOR CAPACITOR MODEL

```

clear
h=0.1; %step
xl=5; %x axis length,cm
yl=20; %y axis length, cm
K=[1 3 10 100];
d=0; %distance between insulator and conductive material

Vol(xl/h,yl/h)=0;

m=1; %iteration mark
DF=0.005; %absolute error for iteration
phi=Vol;
transit=phi;
w=1.64; %relaxation factor
n=0; %mark

while m>0
    for j=yl/h:-1:1 %horizontal number
        for i=xl/h:-1:1 %vertical number
            if i==1 && j>1 && j<yl/h
                %Nphi(i,j)=0;
                Nphi(i,j)=0.25*(2*phi(i+1,j)+phi(1,j+1)+phi(1,j-1)); %AC edge difference equation
            elseif i==xl/h && j>1 && j<yl/h
                %Nphi(i,j)=0;
                Nphi(i,j)=0.25*(2*phi(i-1,j)+phi(i,j+1)+phi(i,j-1)); %BD edge difference equation
            elseif j==yl/h %top boundary condition
                Nphi(i,j)=40;
            elseif j==1 %bottom boundary condition
                Nphi(i,j)=0;
            elseif i>1 && i<xl/h && j==(0.5-d/2)*yl/h
                Nphi(i,j)=0.25*(2/(1+K)*phi(i,j-1)+phi(i+1,j)+2*K/(1+K)*phi(i,j+1)+phi(i-1,j));
            elseif i>1 && i<xl/h && j==(0.5+d/2)*yl/h
                Nphi(i,j)=0.25*(2/(1+K)*phi(i,j+1)+phi(i+1,j)+2*K/(1+K)*phi(i,j-1)+phi(i-1,j));
            %elseif i>1 && i<xl/h && j>(0.5-d/2)*yl/h && j<(0.5+d/2)*yl/h %conductor inside
                %Nphi(i,j)=phi(i,j+1);
            else
                phi4(i,j)=0.25*(phi(i+1,j)+phi(i,j+1)+phi(i-1,j)+phi(i,j-1));
                Nphi(i,j)=phi(i,j)+w*(phi4(i,j)-phi(i,j)); %inside points
            end
            phi(i,j)=Nphi(i,j);

        end
    end

    dif=abs(phi-transit);
    DFt=max(max(dif))
    if DFt<DF
        m=0;
    end
    transit=phi;
    n=n+1
end

```



```
Final=fliplr(flipud(phi)); %turn determinant to x-y system
```

```
P=Final(y1/h:-1:1,floor(x1/h/2));  
%plot(P)%potential curve
```

```
xaxle=1:100/(y1/h):100  
EF=diff(P);plot(xaxle,EF,'LineWidth',3)%EF curve  
xlabel('distance from bottom to top, percentage','FontSize',24);  
ylabel('Electric Field','FontSize',24);  
set(gca,'FontSize',20);
```

APPENDIX B

CODE FOR RAPTOR-INSULATOR MODEL

```

clear
h=0.1; %step
xl=100; %x axis length,inch
yl=83; %y axis length

Wg=0.3; %width of bird guard

Pi=4; %insulator relative permittivity
Pm=10000; %raptor muscle
Pb=1000; %raptor bone
Pf=100; %raptor feather
Pg=10; %raptor guard

Vol(xl/h,yl/h)=0; % set matrix size

m=1; %iteration mark
DF=0.0005; %absolute error for iteration
n=0; %mark
phi=Vol;
transit=phi;

w=1.9774; %relaxation factor

while m>0
    for j=yl/h:-1:1 %horizontal number
        for i=xl/h:-1:1 %vertical number
            if j==1 %bottom boundary
                Nphi(i,j)=0;
            elseif j==yl/h %top boundary
                Nphi(i,j)=0;
            elseif i==xl/h && j>1/h && j<yl/h %right edge
                Nphi(i,j)=0;
            elseif i=0.1 && j>1/h && j<yl/h %pole edge difference equation 1~10/h
                Nphi(i,j)=0;
            elseif i>=80.4/h && i<=83.4/h && j<=36.3/h && j>=39.3/h %conductor
                Nphi(i,j)=69/sqrt(3);

            elseif i>=9/h && i<=46.5/h && j==48.8/h % upper interface of air
and insulator
                Nphi(i,j)=0.25*(2/(1+Pi)*phi(i,j+1)+phi(i+1,j)+2*Pi/(1+Pi)*phi(i,j-1)+phi(i-1,j));
            elseif i>=53.5/h && i<91/h && j==48.8/h % upper interface of air
and insulator
                Nphi(i,j)=0.25*(2/(1+Pi)*phi(i,j+1)+phi(i+1,j)+2*Pi/(1+Pi)*phi(i,j-1)+phi(i-1,j));
            elseif i>=1/h && i<91/h && j==41.2/h % lower interface of air and
insulator
                Nphi(i,j)=0.25*(2/(1+Pi)*phi(i,j-1)+phi(i+1,j)+2*Pi/(1+Pi)*phi(i,j+1)+phi(i-1,j));

```

```

elseif i==91/h && j>=47.5/h && j<=48.8/h % insulator and bird
interface
Nphi(i,j)=0.25*(2/(1+K1)*phi(i-1,j)+phi(i,j+1)+2*K1/(1+K1)*phi(i+1,j)+phi(i,j-1));
elseif i==91/h && j>=41.2/h && j<42.5/h
Nphi(i,j)=0.25*(2/(1+Pi)*phi(i+1,j)+phi(i,j+1)+2*Pi/(1+Pi)*phi(i-1,j)+phi(i,j-1));

elseif i>(1+Wg)/h && i<=46.5/h && j==71.8/h
Nphi(i,j)=0.25*(2/(1+Kb)*phi(i,j+1)+phi(i+1,j)+2*Kb/(1+Kb)*phi(i,j-1)+phi(i-1,j));
elseif i>=53.5/h && i<=99/h && j==71.8/h
Nphi(i,j)=0.25*(2/(1+Kb)*phi(i,j+1)+phi(i+1,j)+2*Kb/(1+Kb)*phi(i,j-1)+phi(i-1,j)); %bird
boundary #1
elseif i>=46.5/h && i<=53.5/h && j==78.8/h
Nphi(i,j)=0.25*(2/(1+Kb)*phi(i,j+1)+phi(i+1,j)+2*Kb/(1+Kb)*phi(i,j-1)+phi(i-1,j)); %bird
boundary #2
elseif i>=(9+Wg)/h && i<=46.5/h && j==54.8/h
Nphi(i,j)=0.25*(2/(1+Kb)*phi(i,j-1)+phi(i+1,j)+2*Kb/(1+Kb)*phi(i,j+1)+phi(i-1,j));
elseif i>=53.5/h && i<=91/h && j==54.8/h
Nphi(i,j)=0.25*(2/(1+Kb)*phi(i,j-1)+phi(i+1,j)+2*Kb/(1+Kb)*phi(i,j+1)+phi(i-1,j)); %bird
boundary #3
elseif i==46.5/h && j>71.8/h && j<78.8/h
Nphi(i,j)=0.25*(2/(1+Kb)*phi(i-1,j)+phi(i,j+1)+2*Kb/(1+Kb)*phi(i+1,j)+phi(i,j-1));
elseif i==46.5/h && j>48.8/h && j<54.8/h
Nphi(i,j)=0.25*(2/(1+Kb)*phi(i-1,j)+phi(i,j+1)+2*Kb/(1+Kb)*phi(i+1,j)+phi(i,j-1)); %bird
boundary #4
elseif i==53.5/h && j>71.8/h && j<78.8/h
Nphi(i,j)=0.25*(2/(1+Kb)*phi(i+1,j)+phi(i,j+1)+2*Kb/(1+Kb)*phi(i-1,j)+phi(i,j-1));
elseif i==53.5/h && j>48.8/h && j<54.8/h
Nphi(i,j)=0.25*(2/(1+Kb)*phi(i+1,j)+phi(i,j+1)+2*Kb/(1+Kb)*phi(i-1,j)+phi(i,j-1)); %bird
boundary #5
elseif i>(1+Wg)/h && i<(9+Wg)/h && j==48.8/h
Nphi(i,j)=0.25*(2/(1+K1)*phi(i,j-1)+phi(i+1,j)+2*K1/(1+K1)*phi(i,j+1)+phi(i-1,j)); %bird
boundary #6
elseif i==99/h && j>=47.5/h && j<71.8/h
Nphi(i,j)=0.25*(2/(1+Kb)*phi(i+1,j)+phi(i,j+1)+2*Kb/(1+Kb)*phi(i-1,j)+phi(i,j-1)); %bird
boundary #7
elseif i>46.5/h && i<53.5/h && j==48.8/h
Nphi(i,j)=0.25*(2/(1+K1)*phi(i,j-1)+phi(i+1,j)+2*K1/(1+K1)*phi(i,j+1)+phi(i-1,j)); %bird
boundary #8
elseif i==(9+Wg)/h && j>48.8/h && j<54.8/h
Nphi(i,j)=0.25*(2/(1+Kb)*phi(i+1,j)+phi(i,j+1)+2*Kb/(1+Kb)*phi(i-1,j)+phi(i,j-1)); %bird
boundary #9
elseif i==91/h && j>48.8/h && j<54.8/h
Nphi(i,j)=0.25*(2/(1+Kb)*phi(i-1,j)+phi(i,j+1)+2*Kb/(1+Kb)*phi(i+1,j)+phi(i,j-1)); %bird
boundary #10
elseif i>96/h && i<99/h && j==47.5/h
Nphi(i,j)=0.25*(2/(1+Kb)*phi(i,j-1)+phi(i+1,j)+2*Kb/(1+Kb)*phi(i,j+1)+phi(i-1,j)); %bird
boundary #11

elseif i==(1+Wg)/h && j>=48.8/h && j<=71.8/h
Nphi(i,j)=0.25*(2/(1+K2)*phi(i-1,j)+phi(i,j+1)+2*K2/(1+K2)*phi(i+1,j)+phi(i,j-1)); %guard
boundary #12
elseif i==(1+Wg)/h && j>=71.8/h && j<=80/h
Nphi(i,j)=0.25*(2/(1+Kg)*phi(i+1,j)+phi(i,j+1)+2*Kg/(1+Kg)*phi(i-1,j)+phi(i,j-1)); %guard

```

```

boundary #13
    elseif i>=1/h && i<(1+Wg)/h && j==48.8/h
        Nphi(i,j)=0.25*(2/(1+K3)*phi(i,j-1)+phi(i+1,j)+2*K3/(1+K3)*phi(i,j+1)+phi(i-1,j)); %guard
boundary #14
    elseif i>=1/h && i<(1+Wg)/h && j==80/h
        Nphi(i,j)=0.25*(2/(1+Kg)*phi(i,j+1)+phi(i+1,j)+2*Kg/(1+Kg)*phi(i,j-1)+phi(i-1,j)); %guard
boundary #15

    else
        phi4(i,j)=0.25*(phi(i+1,j)+phi(i,j+1)+phi(i-1,j)+phi(i,j-1)); Nphi(i,j)=phi(i,j)+w*(phi4(i,j)-
phi(i,j)); %inside points
    end

    phi=Nphi;
end
end
dif=abs(phi-transit);
D=max(max(dif))
if D<DF
    m=0;
end
transit=phi;
n=n+1
end

%vertical
percent1=[0:45/((41.2/h)):45];
P2=phi((1/h+1),48.8/h:90/h)*1000; %insulator surface
figure(1)
hold on
grid on
plot(percent1,P2,'LineWidth',3)%potential curve
%plot(percent1,P3,'LineWidth',3)%potential curve
xlabel('distance from insulator, cm','FontSize',22);
ylabel('Potential, V','FontSize',22);
set(gca,'FontSize',20);

EF2=diff(P2)/h;
percent2=[0:45/((41.2/h-1)):45];
figure(2)
grid on
hold on
plot(percent2,EF2,'LineWidth',3)%EF curve
xlabel('distance from insulator, cm','FontSize',16);
ylabel('Electric Field, V/cm','FontSize',16);
set(gca,'FontSize',20);

```

APPENDIX C

CODE FOR LEAKGE CURRENT DATA ANALYSIS

```

%%%%%%%%%%%%%%%%%%%%%%%%%%%%%%%%%%%%%%%%%%%%%%%%%%%%%%%%%%
%%%%%%%%%%%%%%%%%%%%%%%%%%%%%%%%%%%%%%%%%%%%%%%%%%%%%%%%%%
% This function is used to plot leakage current and surface resistance
% plot with data recording with Labview through NI USB-6008.
%
% Samplerate : sample rate in Labview, pts/s;
% R      : sensor resistance;
% V      : high voltage, V;
% Type   : determine plot, 1 - Sin waveform leakage current
%         2 - RMS waveform leakage current
%         3 - Surface resistance
% Dur    : duration for RMS, 1 - cycle
%         2 - second
%         3 - minute
%%%%%%%%%%%%%%%%%%%%%%%%%%%%%%%%%%%%%%%%%%%%%%%%%%%%%%%%%%
%%%%%%%%%%%%%%%%%%%%%%%%%%%%%%%%%%%%%%%%%%%%%%%%%%%%%%%%%%
clc
clear all
tic
Samplerate=5000;
R=22.2;
V=289;
Type=3;
Dur=1;
sig=textread('2015-7-15LeakageCurrent_DATA.txt','%f');
%sig=readtable('2015-7-16, 1.75kV LeakageCurrent_DATA');
leng=length(sig);
t=1/Samplerate:1/Samplerate:leng*1/Samplerate;
Time_in_minutes=t(leng)/60 %unit:minutes
Time_in_hours=t(leng)/3600 %unit:hours
sig=sig/R; %current measured
if Type==1
    t=t/60; %transfer to mins
    figure
    plot(t,sig)
    grid
    xlabel('Time (min)')
    ylabel('Leakage Current (A)')
    title('Leakage Current')
    set(gca,'fontsize',20);
    set(get(gca,'title'),'FontSize',20);
    set(get(gca,'xlabel'),'FontSize',20);
    set(get(gca,'ylabel'),'FontSize',20);
elseif Type==2
    if Dur==1 % RMS for cycle
        for i=1:leng/Samplerate*60
            R_M_S(i)=rms(sig((fix((i-1)*(Samplerate/60))+1):fix(i*(Samplerate/60))));
        end
        t=0:1/3600:(leng/Samplerate/60-1/3600); %mins
    elseif Dur==2 % RMS for second
        for i=1:leng/Samplerate
            R_M_S(i)=rms(sig(((i-1)*Samplerate+1):(i*Samplerate)));
        end
        t=0:1/60:(leng/Samplerate/60-1/60);
    elseif Dur==3 % RMS for minute

```

```

    for i=1:fix(leng/Samplerate/60)
        R_M_S(i)=rms(sig((fix((i-1)*(Samplerate*60))+1):fix(i*(Samplerate*60))));
    end
    t=0:1:(leng/Samplerate/60-1);
else
    disp('Duration is wrong!')
end
figure
plot(t,R_M_S)
grid
xlabel('Time (min)')
ylabel('Leakage Current (A)')
title('RMS Leakage Current')
% xlim([0 120])
set(gca,'fontsize',20);
set(get(gca,'title'),'FontSize',20);
set(get(gca,'xlabel'),'FontSize',20);
set(get(gca,'ylabel'),'FontSize',20);
elseif Type==3
    if Dur==1 % RMS for cycle
        for i=1:leng/Samplerate*60
            R_M_S(i)=rms(sig((fix((i-1)*(Samplerate/60))+1):fix(i*(Samplerate/60))));
        end
        t=0:1/3600:(leng/Samplerate/60-1/3600); %mins
        Volt=linspace(V,V,leng/Samplerate*60);
    elseif Dur==2 % RMS for second
        for i=1:leng/Samplerate
            R_M_S(i)=rms(sig(((i-1)*Samplerate+1):(i*Samplerate)));
        end
        t=0:1/60:(leng/Samplerate/60-1/60);
        Volt=linspace(V,V,leng/Samplerate);
    elseif Dur==3 % RMS for minute
        for i=1:fix(leng/Samplerate/60)
            R_M_S(i)=rms(sig((fix((i-1)*(Samplerate*60))+1):fix(i*(Samplerate*60))));
        end
        t=0:1:(leng/Samplerate/60-1);
        Volt=linspace(V,V,leng/Samplerate/60);
    else
        disp('Duration is wrong!')
    end
    figure
    plot(t,Volt./R_M_S)
    grid
    xlabel('Time (min)')
    ylabel('Surface Resistance (ohms)')
    title('Surface Resistance under 2.5 uS/cm contamination')
    % xlim([0 120])
    % ylim([0 8e5])
    set(gca,'fontsize',20);
    set(get(gca,'title'),'FontSize',20);
    set(get(gca,'xlabel'),'FontSize',20);
    set(get(gca,'ylabel'),'FontSize',20);
else
    disp('Type is wrong!')
end
end

```


toc